Molecular Therapy
Original Article

Exosome-Mediated miR-29 Transfer Reduces Muscle Atrophy and Kidney Fibrosis in Mice

Haidong Wang,[1,2,8] Bin Wang,[1,3,8] Aiqing Zhang,[1,4] Faten Hassounah,[1] Yiqi Seow,[5,6] Matthew Wood,[6] Fuying Ma,[1] Janet D. Klein,[1] S. Russ Price,[1,7] and Xiaonan H. Wang[1]

[1]Department of Medicine, Renal Division, Emory University, Atlanta, GA 30322, USA; [2]College of Animal Science and Veterinary Medicine, Shanxi Agricultural University, Taigu, Shanxi 030801, China; [3]Institute of Nephrology, Zhong Da Hospital, Southeast University, Nanjing 210009, China; [4]Department of Pediatric Nephrology, the Second Affiliated Hospital of Nanjing Medical University, Nanjing 210003, China; [5]Molecular Engineering Laboratory, Biomedical Medical Sciences Institutes, Singapore, Singapore; [6]Biotechnology and Biological Sciences Research Council, United Kingdom University of Oxford, Oxford, UK; [7]Department of Biochemistry and Molecular Biology, Brody School of Medicine, East Carolina University, Greenville, NC 27834, USA

Our previous study showed that miR-29 attenuates muscle wasting in chronic kidney disease. Other studies found that miR-29 has anti-fibrosis activity. We hypothesized that intramuscular injection of exosome-encapsulated miR-29 would counteract unilateral ureteral obstruction (UUO)-induced muscle wasting and renal fibrosis. We used an engineered exosome vector, which contains an exosomal membrane protein gene Lamp2b that was fused with the targeting peptide RVG (rabies viral glycoprotein peptide). RVG directs exosomes to organs that express the acetylcholine receptor, such as kidney. The intervention of Exo/miR29 increased muscle cross-sectional area and decreased UUO-induced upregulation of TRIM63/MuRF1 and FBXO32/atrogin-1. Interestingly, renal fibrosis was partially depressed in the UUO mice with intramuscular injection of Exo/miR29. This was confirmed by decreased TGF-β, alpha-smooth muscle actin, fibronectin, and collagen 1A1 in the kidney of UUO mice. When we used fluorescently labeled Exo/miR29 to trace the Exo/miR route *in vivo* and found that fluorescence was visible in un-injected muscle and in kidneys. We found that miR-29 directly inhibits YY1 and TGF-β3, which provided a possible mechanism for inhibition of muscle atrophy and renal fibrosis by Exo/miR29. We conclude that Exo/miR29 ameliorates skeletal muscle atrophy and attenuates kidney fibrosis by downregulating YY1 and TGF-β pathway proteins.

INTRODUCTION

Chronic kidney disease (CKD) is a progressive process that ultimately leads to end-stage renal failure. Muscle wasting and renal fibrosis occur in almost every type of CKD patient and are important factors influencing morbidity and mortality.[1–3] The application of miRNA technology has facilitated studies on the advancement of fibrosis at multiple sites in the body, including kidney.[4,5] A large number of recent studies have confirmed that the levels of many miRNAs are altered in fibrotic kidney. Specifically, transforming growth factor β (TGF-β) induces the expression of miR-21, miR-192, miR-214, and the let7 family, and inhibits of expression of the miR-29 and miR-200 families.[6] All of these miRs have been associated with the fibrotic process. We and others confirmed that CKD reduces miR-29 expression in muscles and kidney.[7,8] Muscle wasting is a serious complication of CKD and contributes substantially to the morbidity and mortality of CKD patients.[1,2] The low expression of miR-29 observed in CKD animals results in elevated expression of the transcription factor Yin Yang 1 (YY1). YY1 inhibits muscle satellite cell proliferation and thereby leads to the development of muscle wasting. YY1 is a pro-fibrotic protein in kidney that upregulates α-SMA and collagen.[9] Knockdown of YY1 protects against silica-induced lung fibrosis.[10]

Studies have revealed that miR-29 has anti-fibrosis activity.[11] The miR-29 family expression is decreased after unilateral ureteral obstruction (UUO), which is a widely studied animal obstructive nephropathy model for renal fibrosis.[12] Exogenous application of miR-29, when provided to animals with obstructive and diabetic nephropathies, suppresses progression of kidney fibrosis.[13] The mechanism by which miR-29 exerts its anti-fibrosis effects is thought to involve its ability to inhibit production of several fibrosis-related proteins (http://www.targetscan.org/).

MicroRNAs are biologic markers for diagnosis of diseases and have been tested for treatment of many of these diseases.[14,15] One of the major challenges of using synthetic microRNA for therapy is that exogenously added microRNA is quickly degraded by the high level of ribonuclease activity in plasma. In addition, miRs can be rapidly cleared by bile excretion, renal filtration, or immunologic phagocytosis, leading to minimal accumulation in the tissue targeted for therapeutic treatment.[16] Exosomes are candidates for microRNA carriers because they stabilize microRNA against degradation. Exosomes are a sub-type of extracellular vesicles.[17] They are found in serum, urine, breast milk, saliva, semen, and other biological fluids and are natural

Received 10 July 2018; accepted 11 January 2019;
https://doi.org/10.1016/j.ymthe.2019.01.008.

[8]These authors contributed equally to this work.

Correspondence: Xiaonan H. Wang, MD, Department of Medicine, Renal Division, WMB Room 338C, M/S 1930/001/1AG, 1639 Pierce Drive, Emory University, School of Medicine, Atlanta, GA, 30322, USA.
E-mail: xwang03@emory.edu

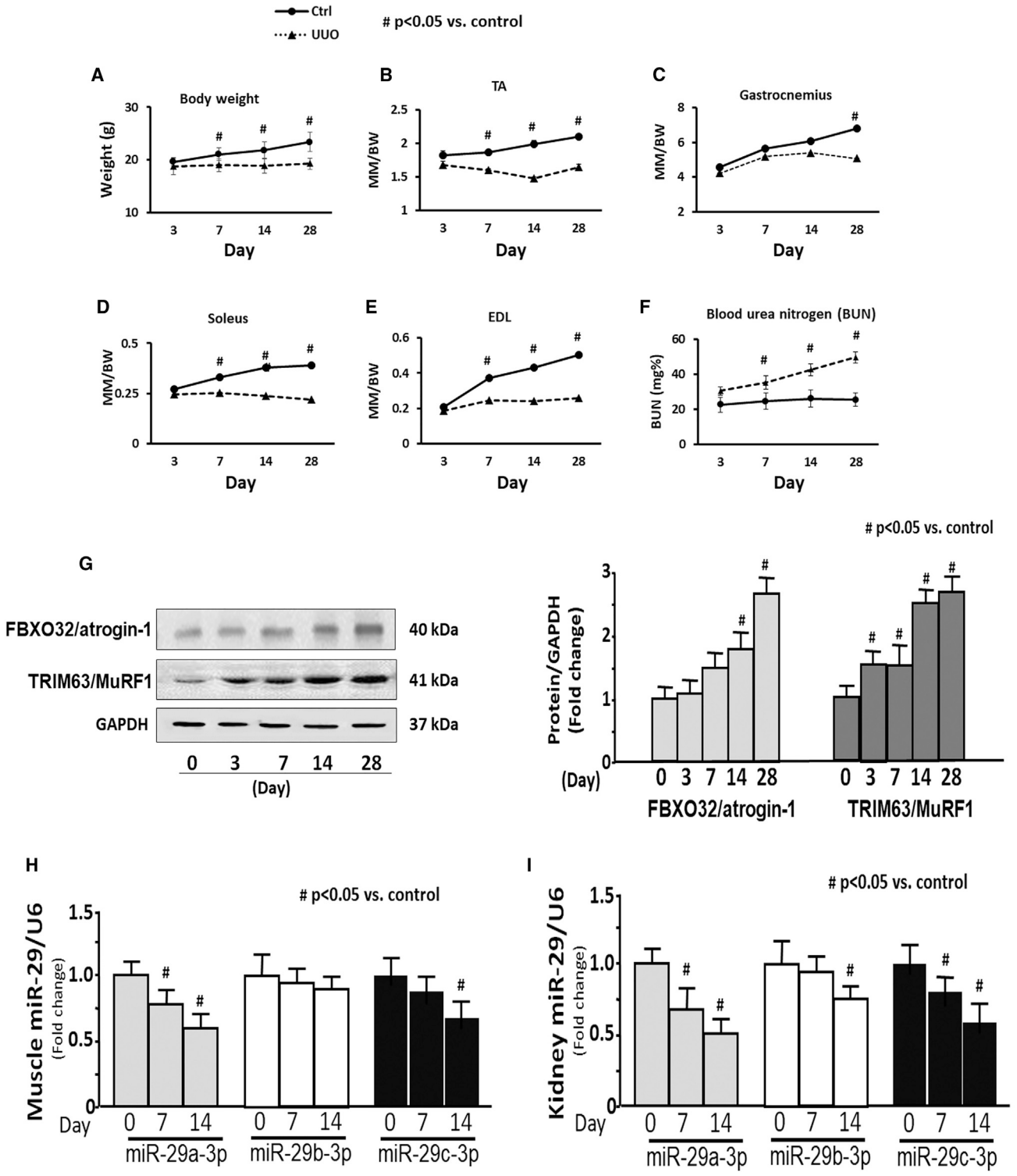

Figure 1. Evidence for Muscle Atrophy in UUO Mice

(A–E) The graphs are body weight (A) and the ratio of skeletal muscle mass to body weight at 3, 7, 14, and 28 days after UUO surgery: (B) tibialis anterior (TA), (C) gastrocnemius, (D) soleus, and (E) extensor digitorum longus (EDL). (F) Blood urea nitrogen measured at different time periods using BLOOD UREA NITROGEN Kinetic Procedure Kit in plasma of control and UUO mice. Results are mean ± SE; n = 9/group; $^{\#}p < 0.05$ versus shams. (G) The two E3 ubiquitin ligase proteins TRIM63/MuRF1 and

(legend continued on next page)

carries of many signaling molecules including proteins, mRNA, and microRNAs.[18,19] They have been used therapeutically to deliver vaccines, chemotherapeutic drugs, and small interfering RNA (siRNA).[20] Exosomes can be less immunogenic, non-cytotoxic, and non-mutagenic to the recipient compared with other gene delivery vehicles.[21]

We hypothesized that intramuscular injected exosome-carried miRs can be transported from skeletal muscle to other damaged organs to rescue their injury. We designed an experimental strategy that produced labeled exosomes containing miR-29 that allowed us to track these exosomes from skeletal muscle to kidney. We used UUO mice, a well-established renal fibrosis model, to test our hypothesis. First, we investigated the effect of exosome/miR29 on muscle wasting in the UUO mouse by examining signaling pathways related with muscle atrophy. Next, we examined the effect of intramuscular injection of exosome/miR-29 on regulation of fibrosis in kidney. Finally, we evaluated the possibility that the mechanism of muscle-kidney communication could involve miR-29 acting through circulating exosomes. Our results suggest a new therapeutic strategy for kidney disease with muscle wasting.

RESULTS

Body Weight and Skeletal Muscle Mass Were Decreased in UUO Mice

To investigate whether protein wasting is related with ureteral obstruction, UUO was induced by ligation of the left ureter in nine male C57BL6 mice. Body and skeletal muscle weights were measured at 3, 7, 14, and 28 days after UUO surgery. The data are presented as the calculated ratio of muscle mass to body weight. Body weight was significantly decreased at 7 days in UUO mice versus sham mice (Figure 1A). The weight ratio of tibialis anterior (TA), extensor digitorum longus (EDL), and soleus were significantly decreased beginning at 7 days (Figures 1B, 1D, and 1E, respectively). Gastrocnemius muscle was significantly decreased at 28 days (Figure 1C). The blood urea nitrogen was significantly raised 7 days after UUO (Figure 1F).

We measured muscle atrophy markers FBXO32/atrogin-1 and TRIM63/MuRF1. Comparing UUO mice with sham mice, the protein level of TRIM63/MuRF1 was significantly increased in TA of UUO beginning at 3 days and was further increased through 28 days. FBXO32/atrogin-1 was significantly increased in the TA of UUO mice at 14 days after UUO and maintained the elevated levels through 28 days (Figure 1G). These data suggest that skeletal muscle wasting occurred in the UUO mice. Our previous study found that miR-29 was decreased in the muscle of CKD mouse.[22] We measured the expression of miR-29a-3p, miR-29b-3p, and miR-29c-3p separately in skeletal muscle and kidney of UUO mice. The expression of miR-29a was decreased in the TA of 7- and 14-day UUO mice versus shams (Figure 1H), and all three miR-29s were decreased in the kidney at 14 days post UUO surgery (Figure 1I).

Intramuscular Injection of Exo/miR29 Counteracts the UUO-Induced Decrease of miR-29a in Muscle

In general, microRNAs that are hosted by exosomes are stable and maintain their integrity,[19] so we used this strategy for microRNA delivery. Using muscle satellite cells as miR-29 exosome donors, we introduced an exosome vector that contains the exosomal membrane protein gene Lamp2b (lysosomal-associated membrane protein 2b) that was fused with the targeting peptide RVG (rabies viral glycoprotein peptide). RVG directs the exosome to organs that express the acetylcholine receptor, such as kidney.[23] Because Lamp2b is ubiquitously expressed on the surface of exosomes, it can bring the targeting peptides (e.g., RVG) to the exosome surface and endow exosome-encapsulated cargo (e.g., miR-29) with targeting ability. We confirmed the miR-29 content of the exosomes from the culture media of the satellite cells by PCR. The expression of miR-29a, miR-29b, and miR-29c was increased in the exosomes isolated from the culture medium by 34-, 21-, and 31-fold, respectively (Figure 2A). The average size of the isolated exosomes was 91 ± 1.9 nm. The yield of exosomes from the culture medium was approximately 1.0×10^{15} particles/mL (Figure S6). The exosome marker Tsg101 was used to verify exosome abundance (Figure 2B).

RVG-exosome/miR-29abc (Exo/miR29) and RVG-exosome/miR-ctrl (Exo/ctrl) were injected into the TA of mice once every week. Exo/miR29 was fluorescently labeled with 1 μmol/L fluorescent lipophilic tracer DiR (Invitrogen) before injection into the TA. The fluorescence intensity and the expression of miR-29 were assessed in the muscle at 14 days after injection. High levels of fluorescence (Exo/miR29) were observed at the injection sites. In addition, fluorescence appeared to accumulate in the right (contralateral) un-injected TA of the UUO mice at higher levels than in the right TA of sham mice (Figure 3A). In muscle injected with Exo/miR29, the expression of miR-29a, miR-29b, and miR-29c in control mice was increased 7.8-fold (miR-29a), 2.9-fold (miR-29b), and 5.4-fold (miR-29c) as determined by PCR analysis. In UUO muscle, the expression of these miRNAs increased 4.6-fold (miR-29a), 2.1-fold (miR-29b), and 4.5-fold (miR-29c), respectively (Figure 3B).

Exo/miR-29 Attenuated UUO-Induced Muscle Loss

Intramuscular injection of Exo/miR29 into the TA of control mice had no effect on body weight and muscle mass. However, this treatment prevented UUO-induced body weight loss. This treatment also reversed the decrease of the soleus, TA, and EDL muscle mass in

FBXO32/atrogin-1 were measured in the TA of sham and UUO mice at 0, 3, 7, 14, and 28 days after UUO surgery. Left: representative western blot of the marker proteins. Right: bar graphs showing the fold change of each protein band compared with levels in sham control mice (represented by 1-fold). All protein band densities have been normalized to the appropriate GAPDH loading control (bars: mean ± SE; n = 4/group; $^{\#}p < 0.05$ versus control). (H and I) Total RNA was extracted from skeletal muscle (H) and kidney (I) of sham (day 0) and UUO mice. The expressions of miR-29a-3p, miR-29b-3p, and miR-29c-3p were assayed by real-time qPCR at 0, 7, and 14 days after UUO surgery. The bar graph shows microRNA from the TA and kidney of each group of mice compared with levels in controls (represented by 1-fold). Results are normalized to U6 (bars: mean ± SE; n = 9/group; $^{\#}p < 0.05$ versus control).

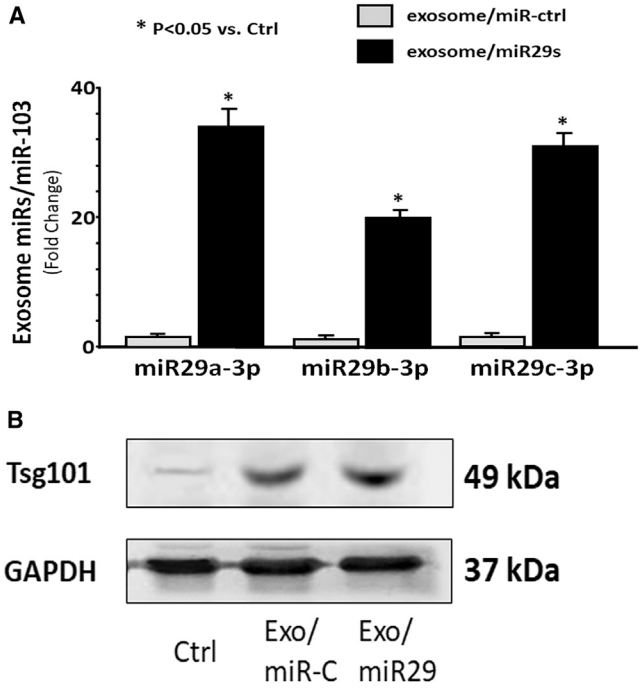

Figure 2. Exo/miR-29 Was Generated from Cultured Cells

(A) The expression of miR-29 in the exosomes isolated from medium. The Lamp2b-RVG vector was transfected into satellite cells using Effectene (transfection reagent; QIAGEN, Valencia, CA, USA). After 6 h of transfection, the cells were transduced with Ad-miR29abc (adenovirus containing miR-29ab1 and miR-29b2c) or Ad-empty (control virus) in extracellular vesicle free serum (EVFS)-containing medium. Fresh EVFS medium was changed after 24 h. All cells were cultured for an additional 48 h to allow exosome release into the medium. The exosomes that are enriched with miR29abc (exosome/miR29) or control (exosome/miR-ctrl) were harvested from culture medium. RNA was isolated from exosomes. The expressions of miR-29a-3p, miR-29b-3p, and miR-29c-3p were assayed by real-time qPCR. The bar graph shows miR expression from the Exo/ctrl (represented by 1-fold) compared with levels in Exo/miR-29s. Results are normalized to miR103a (bars: mean ± SE; n = 6/group; *p < 0.05 versus Exo/ctrl). (B) Exosomes were isolated from the satellite cell culture medium. The protein from cell lysis was used as control. The exosome marker protein, Tsg101, was assayed by western blotting.

UUO mice (Table 1). To confirm this result, we measured muscle cross-sectional area in cryosections of TA at 14 days after UUO surgery. There was no statistical difference of the muscle cross-sectional areas between sham mice treated with Exo/miR-ctrl (2,980 ± 145 μm^2) or Exo/miR29 (2,875 ± 127 μm^2). The overall size distribution of muscle fibers from sham, UUO, and Exo/miR-29-injected UUO mice are shown in Figure 3C. Analysis of the fiber area frequency distribution revealed a clear increase in the percentage of small fibers (a leftward shift) in UUO mice, whereas provision of miR-29 suppressed the leftward shift in the fiber size distribution of UUO mice.

To determine whether the increase in muscle fiber cross-sectional area might reflect increased muscle regeneration in response to Exo/miR29, we measured myogenesis protein markers in muscle with overexpression of miR-29 at 14 days after Exo/miR29 injection. Muscle regeneration-related proteins, myoD, myogenin, and eMyHC, were decreased in UUO muscle, but exogenous miR-29 limited these decreases (Figure 3D). YY1 is a transcription factor that inhibits muscle regeneration.[7] The protein abundance of YY1 is increased in UUO mice; overexpression of miR-29 also retarded this change (Figure 3D). Phosphatase and tensin homolog (PTEN) inhibits myogenesis through the Akt signaling pathway.[24] Exogenous miR-29 decreased PTEN protein abundance in the UUO muscle. Notably, providing miR-29 also repressed the UUO-induced upregulation of the muscle catabolic proteins TRIM63/MuRF1 and FBXO32/atrogin-1 (Figure 3D). These data suggest that injection of Exo/miR29 in skeletal muscle can attenuate UUO-induced body weight loss and muscle atrophy.

Intramuscular Injection of Exo/miR29 Attenuated Renal Fibrosis in UUO Mice

During the UUO study, we found that BLOOD UREA NITROGEN levels of UUO mice with intramuscular injection of Exo/miR29 were significantly decreased compared with Exo/ctrl-injected UUO mice (Figure 4A), suggesting that renal function is improved by Exo/miR29 treatment. To identify whether miR-29 has an impact on UUO-induced renal damage, we assessed kidney fibrosis at 7 days after UUO surgery using Masson's trichrome staining. The intramuscular injection of Exo/miR-29 attenuated the progression of kidney fibrosis in UUO mice (Figure 4B). Comparison of the density of the collagen staining (blue) showed that the area of fibrosis in the UUO kidney with Exo/miR29 was significantly smaller than that of UUO kidney with Exo/ctrl at 3–14 days after UUO (Figure 4C). Alpha-smooth muscle actin (α-SMA) is a molecular signature for myofibroblast activation.[25] The amount of α-SMA was significantly increased in the UUO mice, indicating fibrosis development, but restoration of the level of miR29 significantly decreased the amount of α-SMA in UUO kidney (Figure 4D).

TGF-β is a major inducer of fibrosis.[6] TGF-β1 and TGF-β3 were significantly increased in UUO kidney, as were the extracellular matrix proteins fibronectin, collagen 1A1, collagen 4A1, and vimentin when compared with sham levels at 14 days after Exo/miR-29 injection. Providing miR-29 to skeletal muscle significantly limited the increases of these fibrosis-related proteins, although not returning to sham levels. The exception is vimentin in which miR-29 caused a reduction that did not reach statistical significance. The increase of transcription factor YY1 was also reduced by Exo/miR29 (Figure 4E). These results indicate that intramuscular injection of exogenous miR-29 can attenuate the progression of fibrosis in UUO kidney.

Evidence for Exo/miR-29 in Kidney

To test whether the decreased renal fibrosis that accompanies muscular injection of Exo/miR29 might be related to the increase in circulation of exosome-encapsulated miR-29, we isolated exosomes from the serum of sham and UUO mice that had been injected with Exo/miR29 or Exo/miR-ctrl at 14 days after Exo/miR29 injection. The levels of miR-29a, miR-29b, and miR-29c in serum from both sham and UUO mice were sharply increased relative to mice injected with Exo/miR-ctrl (Figure 5A). A similar increase was seen

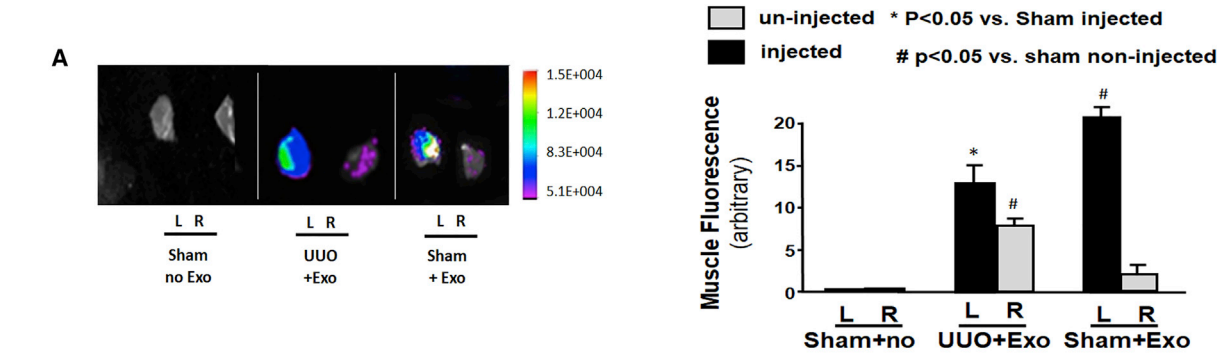

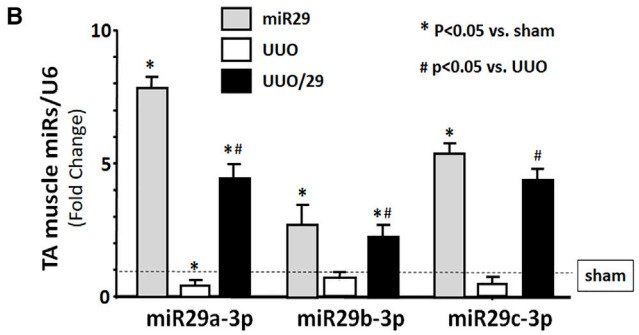

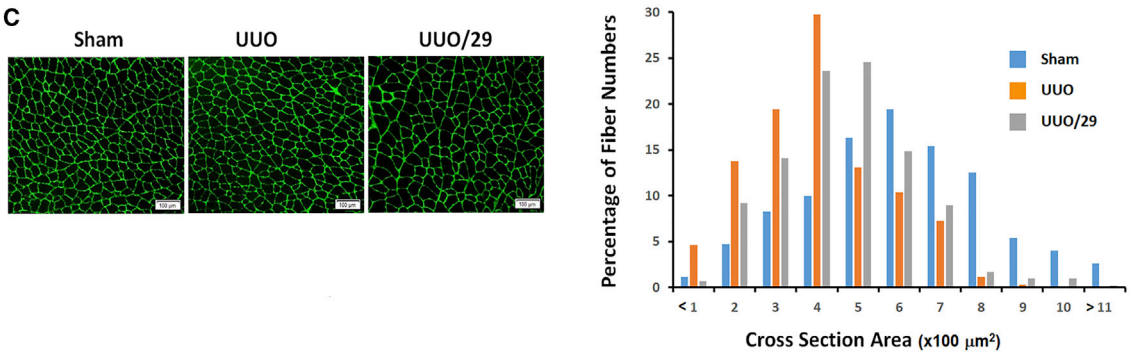

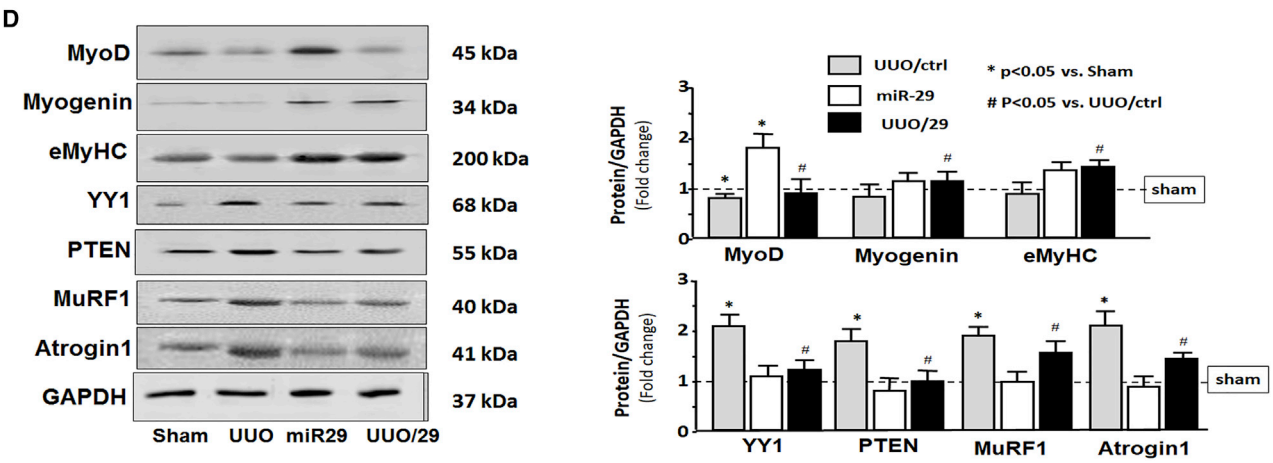

(legend on next page)

Table 1. Body Weights and Muscle Mass of Sham-Operated and UUO Mice

	Sham+Exo/ctrl	Sham+Exo/miR29	UUO+Exo/ctrl	UUO+Exo/miR29
Body weight (g)	26.3 ± 3.5	25.6 ± 2.9	20.5 ± 2.7*	24.2 ± 3.1**
TA (mg)	54.9 ± 1.2	54.7 ± 1.5	46.8 ± 0.9*	50.5 ± 1.4**
Soleus (mg)	9.5 ± 0.9	9.4 ± 1.2	7.1 ± 1.1*	8.2 ± 1.1***
EDL (mg)	10.3 ± 1.2	10.9 ± 1.6	8.2 ± 0.7*	9.5 ± 1.3**

Data are presented as mean ± SE. n = 9/group. *$p < 0.05$ is significant versus sham. **$p < 0.05$ is significant versus UUO+Exo/ctrl.

in the levels of the three miR-29s in kidney tissue from both sham and UUO mice (Figure 5B). Next, we tracked the exosomes containing fluorescently labeled Exo/miR29 using the In-Vivo Xtreme camera system. After intramuscular injection, the fluorescence levels were increased in almost all organs, including non-injected muscle (Figure S1). Interestingly, the UUO kidney has the strongest fluorescent intensity of any of the organs, including the non-UUO kidney (Figure 5C). We confirmed that the concomitant increase of miR-29 in the obstructed kidney was more than in the unobstructed kidney by qPCR (Figure S2). We also found that the protein levels of TGF-β3 and YY1 were significantly decreased in the circulated exosome isolated from the Exo/miR29-treated mice (Figure 5D).

To show that the fluorescence accumulated in the various tissues indicated the presence of Exo/miR29-DiR or Exo/miR-ctrl-DiR, and was not the result of non-specific spreading of unattached dye, we injected free DiR (without exosomes) into TA and looked for fluorescence *in vivo* and *ex vivo*. Fluorescence was observed in legs of the intact mice *in vivo* at 7, 14, and 21 days (Figure S3A). Analysis of organs *ex vivo* showed fluorescence only at the site of injection. At all times, fluorescence was confined in muscle and not detected in other organs, including kidney (Figure S3B). To clarify the impact of RVG targeting, we generated additional exosomes/miR-29 without RVG (FLAG-Exo/miR-29). We injected both FLAG-Exo/miR-29 and RVG-Exo/miR-29 into TA of UUO mice and measured the miR-29 expression in serum, obstructed (UUO) kidney, and the contralateral unobstructed kidney. The expressions of miR-29 in serum exosomes were not significantly different between FLAG- and RVG-miR-29 treatment (Figure S4A). In the contralateral (unobstructed) kidneys, miR-29a expression was significantly increased in RVG-Exo/miR-29-treated mice than FLAG-Exo/miR-29-treated mice (Figure S4B), but not significantly different in miR-29b and miR29-c expression. However, in the UUO kidney, the expressions of miR-29a, miR-29b, and miR-29c were significantly higher in RVG-Exo/miR-29-injected mice than Exo-FLAG/miR-29-injected mice (Figure S4C).

TGF-β3 Is Directly Targeted by miR-29

To explore potential mechanisms by which miR-29 might contribute to anti-fibrosis in kidney, we treated HEK293 cells with TGF-β and Ad-miR29 adenovirus for 24 h. There was no statistical difference between untreated cells and cells treated with miR-control (Figure S5). Treatment with only TGF-β led to increased fibrosis markers in cultured kidney cells evidenced by increasing expression of collagen 1 and αSMC mRNA (Figure 6A). The TGF-β signaling pathway proteins TGF-β1, TGF-β3, and phosphate SMAD2/3 were upregulated with TGF-β treatment. Fibrosis marker proteins collagen 1a1 and αSMC were also increased. In cells also treated with Ad-miR29, all these changes were blocked (Figure 6B). An *in silico* analysis of the 3′ UTR of TGF-β3 predicted a conserved binding site for miR-29 (http://www.targetscan.org/). To experimentally confirm that miR-29 interacts with the TGF-β3 mRNA, the TGF-β3 target site of miR-29 (838–844 nt on Tgfb3 3′ UTR) was cloned into a luciferase reporter construct (pLUC-TGF-β3) and transfected into HEK293 cells. Luciferase activity was measured after 24 h. When transfected cells were also transduced with Ad-miR-29, luciferase activity was decreased, indicating binding of miR-29 to TGF-β3. When cells were transduced with miR-29 in which the binding site had been mutated, the miR-29-mediated decrease was eliminated, indicating no binding (Figure 6C). This result was consistent with the observed decrease in TGF-β3 protein abundance in kidney upon intramuscular injection of Exo/miR29 (Figure 4E). These data suggest that the

Figure 3. Exo/miR-29 Attenuated UUO-Induced Muscle Loss

Mice were injected with exosomes carrying either miR-control or miR-29. (A) Mice were injected in the left TA with Exo/miR29 labeled with 1 μmol/L fluorescent lipophilic tracer DiR at the same time as UUO surgery. The injection was repeated once per week. The fluorescence was assessed in muscle at 14 days after injection. Panels from left to right: sham operated with no exosome injection, UUO mouse at 14 days (twice injection) after DiR∼Exo/miR29 injection, and sham operated with DiR∼exosome injection. In each pair, the left TA received the Exo/miR29 injection and the right did not. Fluorescent images were acquired using a Bruker Small Animal Optical Imaging System (In-Vivo Xtreme II). The white color indicates fluorescence level over maximal measurement limits. The picture with all organs compared is shown in Figure S1. The bar graph compares fluorescence intensity from each muscle (bars: mean ± SE; n = 3/group; *$p < 0.05$ versus sham injected muscle; #$p < 0.05$ versus sham non-injected muscle). (B) Total RNA was isolated from TA of sham plus Exo/miR-ctrl (sham), sham plus Exo/miR29 (miR29), UUO plus Exo/miR-ctrl (UUO), and UUO plus Exo/miR-29 mice (UUO/29). The expressions of miR-29a-3p, miR-29b-3p, and miR-29c-3p were assayed by real-time qPCR. The bar graph shows expression levels of the three miRs in each treatment group compared with levels in sham mice (represented by a line at 1-fold). Results are normalized to U6 (bars: mean ± SE; n = 9/group; *$p < 0.05$ versus sham; #$p < 0.05$ versus UUO). (C) The representative cross-sectional area of TA of sham plus Exo/miR-ctrl (sham), UUO plus Exo/miR-ctrl (UUO), and UUO plus Exo/miR-29 mice (UUO/29). Cryosections of TA were immunostained with anti-laminin antibody. The bar graph shows the frequency distribution of fiber cross-sectional areas in sham (blue), UUO (orange), and UUO/29 (green) mice (data are mean ± SE; n = 6/group; *$p < 0.05$ versus sham; #$p < 0.05$ versus UUO). (D) Shown are representative western blots of the muscle regeneration- and atrophy-related proteins myoD, myogenin, eMyHC, YY1, PTEN, MuRF1, and atrogin1 in muscle lysates from the different treatment groups of mice. All blots were also probed for GAPDH, and all protein band densities have been normalized to their corresponding GAPDH loading control. The bar graph shows the fold change of each protein band compared with levels in sham mice (represented by a line at 1-fold) (bars: mean ± SE; n = 9/group; *$p < 0.05$ versus sham; #$p < 0.05$ versus UUO).

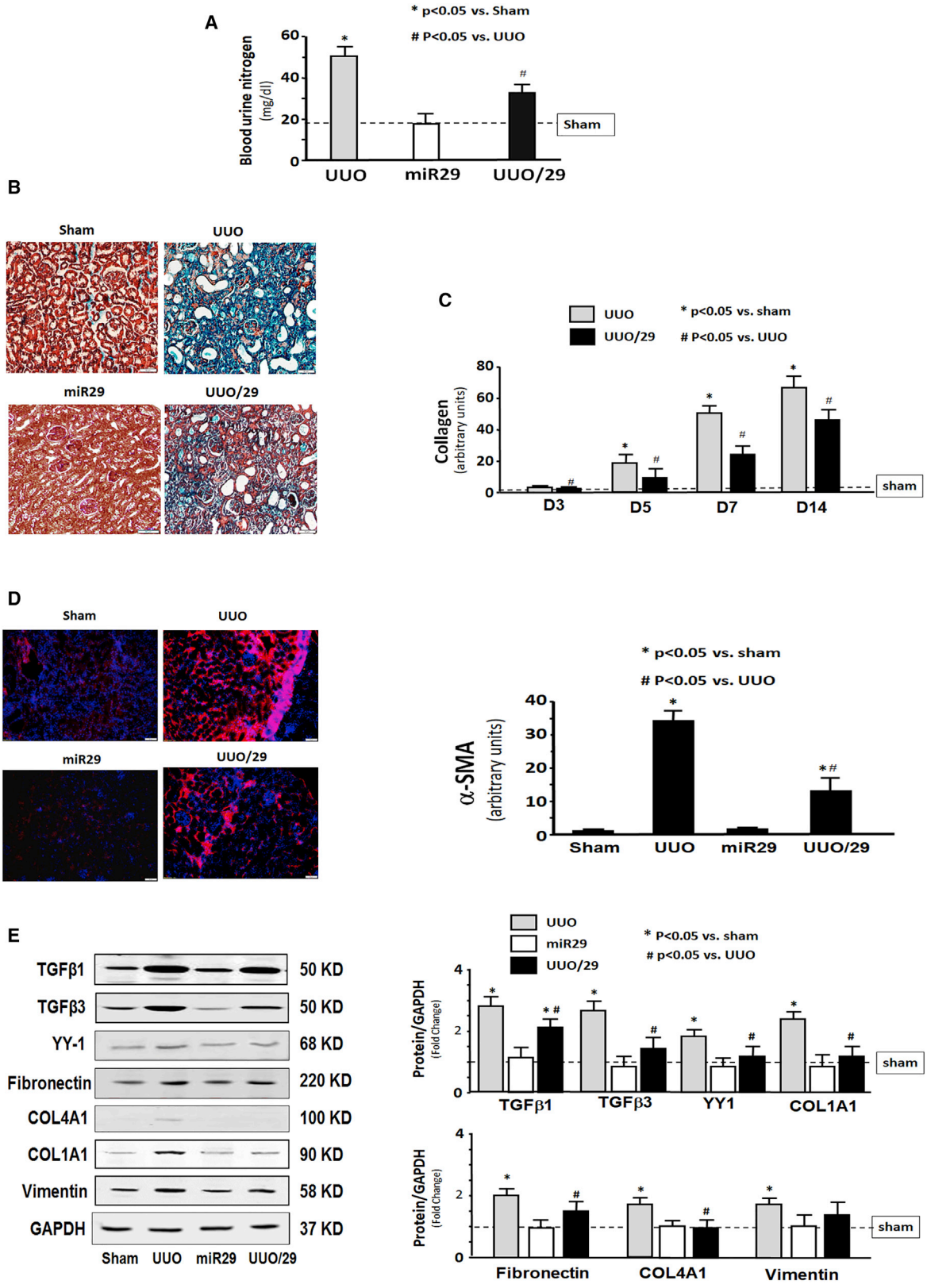

(legend on next page)

decrease in renal fibrosis in miR-29-injected UUO mice may result, in part, from suppressing the expression of TGF-β3.

DISCUSSION

The data from this study provide evidence that injection of exosome-encapsulated miR-29 into the muscle of UUO mice reduced muscle atrophy and attenuated kidney fibrosis by a mechanism that includes downregulation of YY1 and TGF-β3.

Kidney fibrosis results from a number of pro-fibrotic factors. TGF-β and YY1 play an important role in the progress of renal fibrosis. miR-29 has been shown to inhibit YY1,[7] and here we show that it can inhibit TGF-β3. Transcription factor YY1 directly upregulates αSMA and collagen;[9] inhibition of YY1 by miR-29 can limit fibrosis in UUO kidney. TGF-β3 shares 70%–82% homology with TGF-β1 and TGF-β2 at the amino acid level.[26] All three isoforms bind to TGF-β receptor 2, which then recruits TGF-β receptor 1 to activate SMAD-based or non-SMAD-based pathways, resulting in fibrosis. Inhibition of TGF-β3 contributes to the observed decrease in renal fibrosis. YYI and TGF-β3 were decreased in the exosomes in circulation following injection of Exo/miR29, suggesting that miR-29 is actively altering levels of these two factors. More importantly, the level of pro-fibrotic proteins in the kidney tissue was decreased strongly, suggesting that Exo/miR29 was exerting an anti-fibrotic effect through altering YY1 and TGF-β3.

In our earlier publication we treated diabetic mice with a muscle injection of AAV-microRNA and observed that this microRNA was transported from muscle to kidney by exosomes.[27] The current study indicates that kidney fibrosis is reduced when muscle wasting is reduced following treatment using injected exosomes containing miR-29. The downstream kidney benefit suggests that the miR-29 in the injected exosomes is functional. It is possible that when injected into the muscle, some miR-29 enters the circulation, travels to the kidney, and directly inhibits renal fibrosis, and this improvement ameliorates muscle wasting. Whether the Exo/miR29 goes to the kidney directly or indirectly through muscle release, the result is reduction of kidney fibrosis and limiting of muscle loss. Understanding the cause and effect of this process will require further detailed investigation.

The ability to modify the exosome surface to target specific cells for uptake has tremendous therapeutic promise.[28] The engineered exosome vectors that contain RVG target organs that express the acetylcholine receptor such as kidney and liver.[23,29] Given the large perfusion of these organs with blood containing the exosomes, it is not unexpected that exosomes would bind in both organs. Particularly, liver has two blood supplies, the hepatic portal vein and the hepatic arteries, which results in a high blood volume through this organ.[30] In addition, Kupffer cells, also known as stellate cells, are specialized macrophages located in the liver that may have the ability to phagocytose exosomes. This could be the reason that many exosomes accumulate in healthy liver. However, we found that damaged organs, such as UUO kidneys, accumulate more Exo/miR29 than non-injured organs. This tendency to accumulate in damaged tissue suggests that, clinically, treatment with therapeutic exosomes could result in higher levels of therapeutic miRs concentrated at damaged kidney, which could aid in recovery from fibrotic lesions. We posit that the damaged tissue creates a hierarchy for recruitment of exosomes, and the injured kidney induces secretion of inflammatory cytokines, leading to increased capillary permeability, which could be the reason for more exosome uptake.[31]

A limitation of this study is that the follow-up of the treatment was relatively short. Indeed, renal fibrosis in the clinics is a progressive process that is the consequence of most CKDs. Although the treatment tested here in mice produced a decrease in renal fibrosis and muscular atrophy over a 2-week period, the question that remains is whether the beneficial effect would be observed in the long term. Although promising as a potential therapy, a longer-term analysis should be the focus of a future study.

In conclusion, injection of an engineered exosome containing miR-29 into TA in a mouse with UUO results in reduction of muscle wasting, but also reduction of kidney fibrosis. The mechanism by which this benefit was achieved involves limiting the TGF-β signaling pathway. This study shows that engineered exosomes carrying microRNA can be introduced into muscle and then target multiple tissues offering potential treatment strategies for diseases with multiple organ failure.

MATERIALS AND METHODS

Animals and Unilateral Ureteral Obstruction Model

These experiments were approved by the Emory University Institutional Animal Care and Use Committee (IACUC; protocol 4000152). Two-month-old mice (C57BL/6J) from Jackson Laboratories (Bar

Figure 4. Intramuscular Injection of Exo/miR29 Attenuated Renal Fibrosis in the Kidney of UUO Mice

Mice were injected with exosomes carrying either miR-control or miR-29. (A) Blood urea nitrogen was measured in sham plus Exo/miR-ctrl (sham), sham plus Exo/miR29 (miR29), UUO plus Exo/miR-ctrl (UUO), and UUO plus Exo/miR-29 mice (UUO/29). The bar graph shows the BLOOD UREA NITROGEN levels in each group compared with levels in sham mice (represented by a line) (bars: mean ± SE; n = 9/group; *p < 0.05 versus sham; #p < 0.05 versus UUO). (B) Shown is representative Masson's trichrome staining of paraffin sections from kidneys of the four treatment groups. (C) The bar graph shows collagen amount in Masson's trichrome staining measured at days 3, 5, 7, and 14. Results show the fold change compared with sham levels represented by a line at 1-fold (bars: mean ± SE; n = 6/group; *p < 0.05 versus control). (D) Representative kidney cryosections in each group were immunostained with anti-alpha smooth muscle actin (α-SMA) antibody. The bar graph shows α-SMA amount measured at day 7. Results show the fold change compared with sham levels defined as 1-fold (bars: mean ± SE; n = 6/group; *p < 0.05 versus control). (E) Shown are representative western blots of fibrosis-related proteins, TGF-β1, TGFβ-3, fibronectin, vimentin, collagen 1α1, collagen 4α1, and YY1, in kidney lysates from different groups of mice. The bar graph shows the fold change of the protein band compared with levels in sham mice represented by a line at 1-fold. All blots were also probed for GAPDH, and all protein band densities have been normalized to their corresponding GAPDH loading control (bars: mean ± SE; n = 9/group; *p < 0.05 versus sham; #p < 0.05 versus UUO).

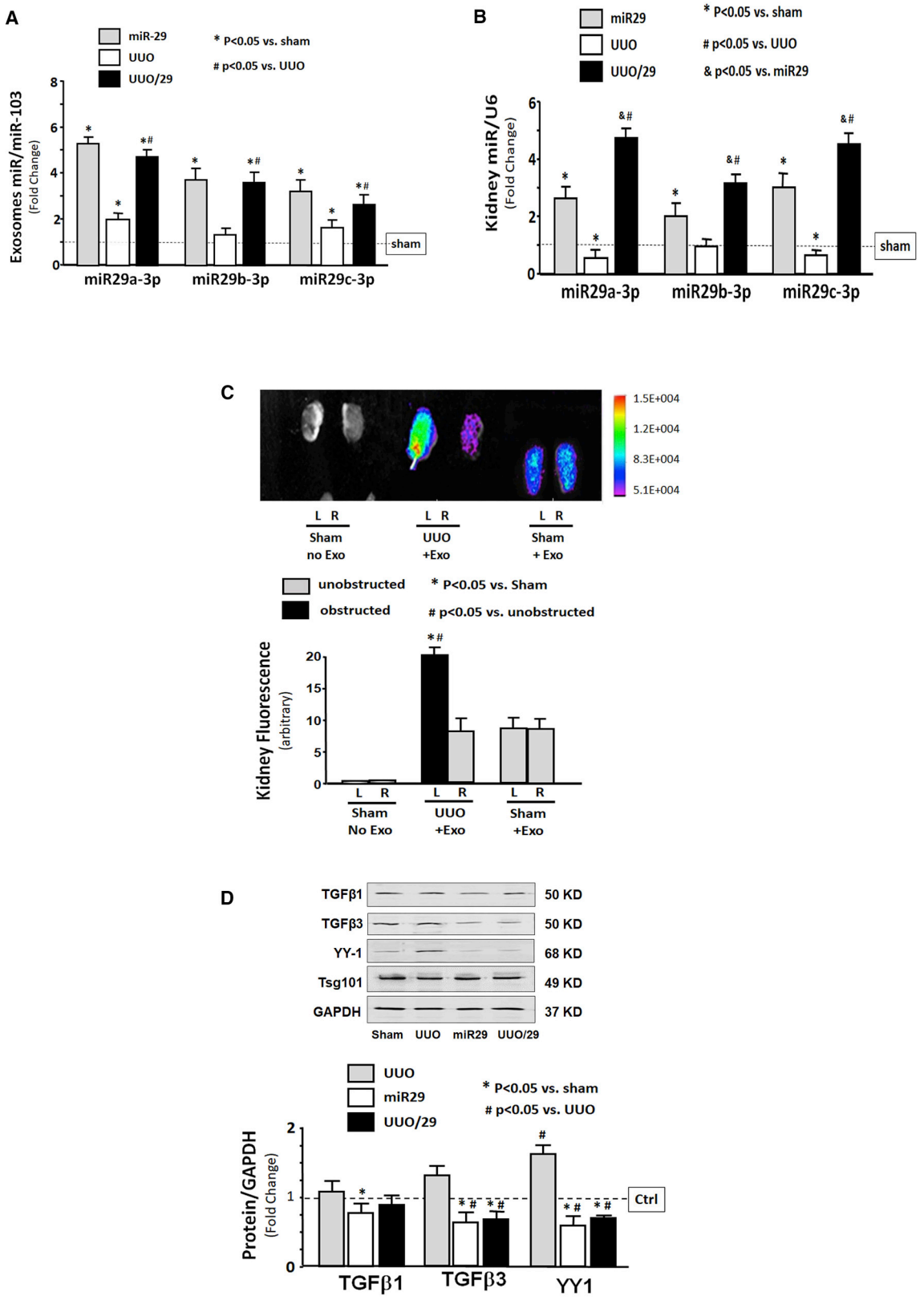

(legend on next page)

Harbor, ME, USA) were used for UUO surgery. The details of the UUO surgery are provided in the Supplemental Materials and Methods. After surgery, the body weight and food taken were measured three times per week. The mice were terminated at 3, 7, 14, and 28 days after the UUO operation. Blood urea nitrogen was measured with a BLOOD UREA NITROGEN Kinetic Procedure Kit (Thermo Electron, Louisville, CO, USA).

Generation of Exosome-Encapsulated miR-29

Primary mouse satellite cells were cultured in growth medium. At 60% confluence, the Lamp2b-RVG vector was transfected into the cells using the Effectene transfection reagent (QIAGEN, Valencia, CA, USA). Six hours after transfection, the cells were transduced with Ad-miR29abc (adenovirus containing miR-29ab1 and miR-29b2c).[7] Control cells were transduced with Ad-empty for production of RVG-exosome-control (Exo/ctrl). Twenty-four hours after transduction, the culture medium was exchanged for a medium with extracellular vesicle free serum (EVFS) and cultured for an additional 48 h to allow exosomes to be released into the medium. The RVG-exosomes enriched with miR-29abc (Exo/miR29) were harvested from culture medium and re-suspended in PBS. Previous study showed that RVG is located on the external exosome membrane.[29]

Exosome Isolation, NanoSight Measurement, and *In Vivo* Imaging

To isolate exosomes, we removed cell debris and non-exosome organelles from either serum (diluted 5× with PBS) or culture medium (undiluted) by centrifugation at 1,000 × *g* for 10 min at 4°C. The supernatant fraction was further centrifuged at 16,000 × *g* for 30 min at 4°C. This second supernatant was sterile filtered through a 0.22-μm filter. Exosomes were pelleted from this filtrate at 120,000 × *g* for 90 min at 4°C (L8-70M ultracentrifuge; Beckman-Coulter, Indianapolis, IN, USA). Exosome pellets were re-suspended in PBS, and protein was quantified using a Bradford protein assay (Bio-Rad, Hercules, CA, USA). Exosome concentration and size (Figure 2B) were measured using a nanoparticle tracking analysis (NanoSight NS300; Malvern Instruments, Westborough, MA, USA). *In vivo* exosome distribution (Figure S1) was determined with the Bruker Small Animal Optical Imaging System (In-Vivo Xtreme II; Bruker, Billerica, MA, USA).

Western Blot and Antibodies

Equal amounts of protein from TA or whole kidney were used for western blots.[32,33] We used 50 μg for exosome protein loading and 20 μg for the skeletal muscle and kidney. Protein bands were scanned and quantified using the Li-COR Odyssey infrared scanning system (Li-COR Biosciences, Lincoln, NE, USA). Primary antibodies (1:1,000 dilution except indicated): Akt (C67E7), p-Akt Ser473(D9E), FoxO1(75D8), p-FoxO1(Thr24, #9464), pSmad2/3(D27F4), and Smad2/3(D7G7) were from Cell Signaling (Danvers, MA, USA). Type I collagen (catalog no. [Cat#] 131001; Southern Biotech, Birmingham, AL, USA), PTEN (Cat# FL-403), and TSG 101 (C2) were from Santa Cruz (Santa Cruz, CA, USA); TGF-β (Cat# AB-100-NA) was from R&D Systems (Minneapolis, MN, USA); and GAPDH (Cat# MAB374) was from Millipore (Burlington, MA, USA). COL4A1 (ab6586), GFP (ab1218), TRIM63/MuRF1 (ab77577), and FBXO32/atrogin-1 (ab168372) were from Abcam (Cambridge, MA, USA); αSMA (A2547), fibronectin (F3648), and vimentin (V2258) were from Sigma-Aldrich (St. Louis, MO, USA). Protein bands were scanned and quantified using the Li-COR Odyssey infrared scanning system (Li-COR Biosciences, Lincoln, NE, USA).

RNA Extraction and Real-Time qPCR

Exosomal RNA was isolated using an miRNeasy kit (217004; QIAGEN Sciences, Germantown, MD, USA) and quantified using a NanoDrop spectrophotometer (Thermo Scientific, Wilmington, DE, USA). The miR primers were purchased from Exiqon. Real-time qPCR was performed with the ExiLENT SYBR green master mix (Exiqon Cat# 203421). The detail protocol on RT-PCR can be found in the Supplemental Materials and Methods.[34,35] The detailed measurement of mRNA repression is in the Supplemental Materials and Methods, and the primer sequence is in Table 2.

Culture of Primary Muscle Satellite Cells

Satellite cells were isolated from the hindlimb muscles of 4-month-old mice. A Skeletal Muscle Dissociation Kit (130-098-305; MACS; Miltenyi Biotec, Auburn, CA, USA) was used to dissociate muscle tissue into cell suspensions, and a Satellite Cell Isolation Kit (130-104-267; MACS) was used to isolate satellite cells. Primary mouse satellite cells were cultured in Ham's F-10 Nutrient Mixture medium (Invitrogen)

Figure 5. Evidence of Exo/miR-29 in Kidney

Mice were injected with exosomes carrying either miR-control or miR-29. (A and B) Total RNA was isolated from (A) serum exosomes and (B) whole kidney of sham plus Exo/miR-ctrl (sham), sham plus Exo/miR29 (miR29), UUO plus Exo/miR-ctrl (UUO), and UUO plus Exo/miR-29 mice (UUO/29). The expressions of miR-29a-3p, miR-29b-3p, and miR-29c-3p were assayed by real-time qPCR. The bar graphs show miR expression of each group of mice compared with levels in control mice (represented by a line at 1-fold). (A) Bars represent mean ± SE; n = 6/group. *$p < 0.05$ versus sham; $^{\#}p < 0.05$ versus UUO. Results are normalized to miR103a. (B) Bars represent mean ± SE; n = 6/group. *$p < 0.05$ versus sham; $^{\#}p < 0.05$ versus UUO; $^{\&}p < 0.05$ versus miR29. Results are normalized to U6. (C) Mice were injected in the left TA with Exo/miR-29 labeled with 1 μmol/L fluorescent lipophilic tracer DiR at the same time as UUO surgery. The injection was repeated once per week. Shown are representative fluorescent kidney images at 14 days that were acquired using a Bruker Small Animal Optical Imaging System. Panels from left to right: sham operated with no exosome injection, UUO mouse with exosome injection, and sham-operated mouse with exosome injection. The bar graph shows fluorescence intensities of the kidneys. The original whole picture was shown in Figure S1 (bars: mean ± SE; n = 3/group; *$p < 0.05$, UUO versus sham mouse; $^{\#}p < 0.05$, UUO mouse obstructed kidney versus UUO mouse unobstructed kidney). (D) Circulation exosomes from different group mice were solubilized in Laemmli sample buffer, and fibrosis-related proteins TGF-β1, TGF-β3, and YY1 were analyzed by western blot. All blots were also probed for GAPDH, and all protein band densities have been normalized to their corresponding GAPDH loading control. The bar graph shows the fold change of each protein band compared with levels in control plus Exo/miR-ctrl (represented by a line at 1-fold) (bars: mean ± SE; n = 9/group; *$p < 0.05$ versus UUO; $^{\#}p < 0.05$ versus sham).

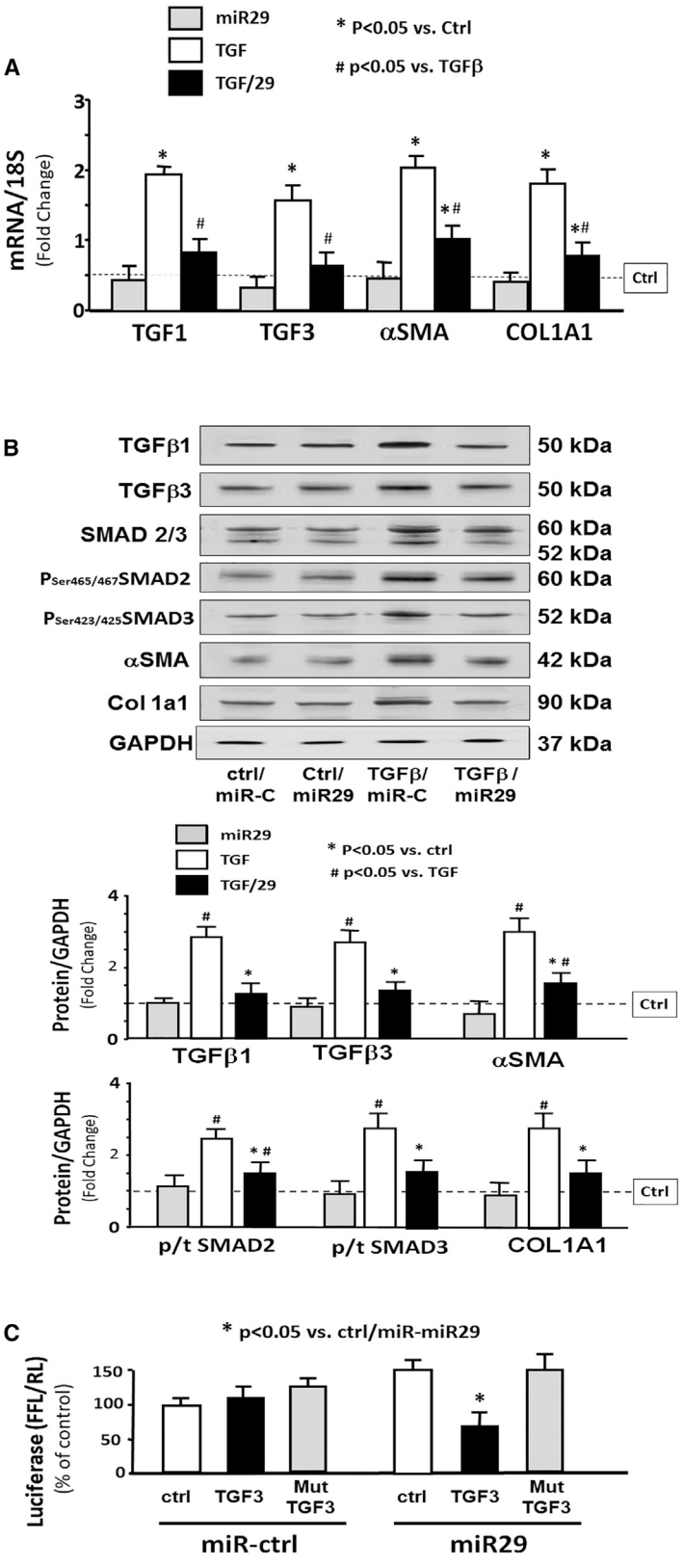

Figure 6. TGF-β3 Is Directly Targeted by miR-29

(A) Cultured HEK293 cells were treated with Ad-miR-ctrl (ctrl), Ad-miR29 (miR29), Ad-miR-ctrl + 10 ng/mL TGF-β (TGF-β), and Ad-miR-29 + TGF-β (TGF-β/29). Total RNA was extracted from the cells 24 h after treatment. The expressions of TGF-β1, TGF-β3, α-SMA, and collagen 1A1 (COL1A1) were assayed by real-time qPCR. The bar graph shows mRNA from the cells of each group compared with levels in Ad-miR-ctrl (represented by a line as 1-fold). Results are normalized to 18S (bars: mean ± SE; n = 9/group; *p < 0.05 versus Exo/miR-ctrl; #p < 0.05 versus Exo/miR-ctrl + TGF-β). (B) The fibrosis-related proteins TGF-β1, TGF-β3, SMAD 2/3, and phosphorylated SMAD 2/3 (pSer465 or pSer423 SMAD2/3) and collagen 1A1 were measured by western blotting in HEK293 cell lysates following the treatments described in (A). The bar graph shows total proteins or the ratios of each phospho-SMAD to total SMAD protein (p/t). All blots were also probed for GAPDH, and all protein band densities have been normalized to their corresponding GAPDH loading control. The fold change of the protein band or ratio is compared with levels in control plus Exo/miR-ctrl (represented by a line at 1-fold) (bars: mean ± SE; n = 9/group; *p < 0.05 versus UUO; #p < 0.05 versus sham). (C) Luciferase assessment of miR-29 binding on 3′ UTR of TGF-β3. HEK293 cells were transfected with luciferase control plasmid (pLuc-ctrl), a plasmid containing the 3′ UTR of TGF-β3 (pMIR-TGF-β3/838-844), and a plasmid containing mutated 3′ UTR of TGF-β3 (pMIR-mut-TGF-β3). Cells were co-transfected with renilla luciferase. After 6 h, cells were transduced with adenovirus containing miR29 (miR29) or control virus (miR-ctrl), and luciferase activity was assayed after an additional 24 h. Luciferase activity in cells that received the pLuc-ctrl with miR-ctrl was designated as 100%. The other bars show the response to miR-29 expressed as a percent of the control. Triplicate determinations were made in each condition, and each experiment was repeated a total of three times; the firefly luciferase (FFL) results were normalized by renilla luciferase (RL) activity. Data are mean ± SE; n = 9. *p < 0.05 versus pLuc+Ad-ctrl.

Table 2. Primer Sequences

Name	Sequences	Amplicon	Code
TGF-β1	forward: 5′-AGGTCACCCGCGTGCTAAT-3′	306	NM_011577
	reverse: 5′-TCAGCCACTGCCGGACAACT-3′		
α-SMA	forward: 5′-GAGAAGCCCAGCCAGTCG-3′	240	NM_007392.3
	reverse: 5′-CTCTTGCTCTGGGCTTCA-3′		
TGF-β3	forward: 5′-TGAGTTCATGCACCCTCTTG-3′	170	NM_009368.3
	reverse: 5′-AGGACTACCAGAGCCCTTTG-3′		
COL1A1	forward: 5′-GTCCCAACCCCCAAAGAC-3′	78	NM_007742.3
	reverse: 5′-CATCTTCTGAGTTTGGTGATACGT-3′		
18S	forward: 5′-CCA GAG CGA AAG CAT TTG CCA AGA-3′	101	X00686
	reverse: 5′-TCG GCA TCG TTT ATG GTC GGA ACT-3′		

with 20% fetal bovine serum, 100 U/mL penicillin, and 100 μg/mL streptomycin (growth medium). Myotube differentiation was inhibited by the addition of 5 ng/mL human β-fibroblast growth factor (FGF; Atlanta Biologicals, Atlanta, GA, USA) to the media. Primary mouse satellite cells were differentiated to myotubes by removing FGF. The detailed protocol on satellite cells culture can be found in the Supplemental Materials and Methods.[36,37] The Effectene transfection reagent (QIAGEN, Valencia, CA, USA) was used to introduce the targeting vectors.

Muscle and Kidney Histology

Kidneys were fixed in 3.7% formaldehyde/PBS (pH 7.4) and dehydrated, paraffin embedded, and sectioned. Masson's trichromatic staining was performed with a Masson's modified IMEB stain kit (K7298; IMEB, San Marcos, CA, USA). Images were visualized with an Olympus 1X 51 inverted microscope and captured by DP73-1-51-17MP color camera.[27] Collagen (blue color) in kidney was measured using the CellSens Dimension 1.9 Software (Olympus, Melville, NY, USA), and color density was calculated as the average from 10 individual fields. For skeletal muscle immunohistology, muscles were embedded in Tissue Freezing Media (Cat# H-TFM; Fisher, Pittsburgh, PA, USA) by immersing in isopentane cooled in dry ice. Cross sections (10 mm) from the mid-belly of different muscles were mounted on gelatin-coated slides and fixed in 4% paraformaldehyde. Muscle fiber cross-sectional area was determined in TA using an anti-laminin antibody (1:50 dilution; Sigma-Aldrich), and at least 500 individual myofibers per muscle were measured. All histological analysis was performed in a blinded fashion.

Luciferase Reporter Assay and Transfection

Effectene transfection reagent was used for transfection (QIAGEN, Valencia, CA, USA). Firefly and Renilla luciferase activities were measured by dual-luciferase assays (Promega) using TD-20/20 Luminometer (Turner Designs, Sunnyvale, CA, USA).[36] The luciferase report vectors (pMIR-REPORT Luciferase) were purchased from Applied Biosystems (Waltham, MA, USA), and constructs were made by Emory Integrated Genomics Core.

Statistical Analysis

Data were presented as mean ± SE. To identify significant differences between two groups, we made comparisons by using the Student's t test. When multiple treatments were compared, ANOVA was performed with a post hoc analysis by the Student-Newman-Keuls test. The Shapiro-Wilk test for non-normality of the ANOVA residuals was not statistically significant. The relationship between muscle and kidney fluorescence intensity was calculated by linear regression modeling. Differences with p values <0.05 were considered significant.

SUPPLEMENTAL INFORMATION

Supplemental Information includes six figures and Supplemental Materials and Methods and can be found with this article online at https://doi.org/10.1016/j.ymthe.2019.01.008.

AUTHOR CONTRIBUTIONS

This project was designed by X.H.W., H.W., and B.W. Experiments were performed by H.W., B.W., A.Z., F.H., and F.M. Data were analyzed by X.H.W., H.W., and B.W. The manuscript was prepared by X.H.W., H.W., and B.W. The manuscript was edited by X.H.W., J.D.K., and S.R.P. Y.S. and M.W were consultants and provided exosome vectors.

CONFLICTS OF INTEREST

The authors declare no competing interests.

ACKNOWLEDGMENTS

Research reported in this publication was supported by the National Institute of Arthritis and Musculoskeletal and Skin Diseases (NIAMS) of the NIH (award R01 AR060268 to X.H.W.), the American Heart Association Bayer Discover and Innovation (grant 17IBDG33780000 to X.H.W.), the National Natural Science Foundation of China (grant 31772690 to H.W.), an NIH/NIDDK grant (R01DK095610 to S.R.P.), and VA MERIT grants (I01-BX001456 to S.R.P.). This research project was also supported in part (microRNA deep sequencing) by the Genomics core of Yerkes National Primate Research Center under an NIH award (ORIP/OD

P51OD011132). The pLamp2b-RVG vectors and control vectors were gifts from Drs. Matthew Wood and Yiqi Seow at the University of Oxford, UK. The content is solely the responsibility of the authors and does not necessarily reflect the official views of the NIH, the Department of Veterans Affairs, or the US Government.

REFERENCES

1. Avram, M.M., and Mittman, N. (1994). Malnutrition in uremia. Semin. Nephrol. *14*, 238–244.
2. Griffiths, R.D. (1996). Muscle mass, survival, and the elderly ICU patient. Nutrition *12*, 456–458.
3. Eddy, A.A., and Neilson, E.G. (2006). Chronic kidney disease progression. J. Am. Soc. Nephrol. *17*, 2964–2966.
4. Gomez, I.G., Nakagawa, N., and Duffield, J.S. (2016). MicroRNAs as novel therapeutic targets to treat kidney injury and fibrosis. Am. J. Physiol. Renal Physiol. *310*, F931–F944.
5. Meng, X.M., Tang, P.M., Li, J., and Lan, H.Y. (2015). TGF-β/Smad signaling in renal fibrosis. Front. Physiol. *6*, 82.
6. Meng, X.M., Nikolic-Paterson, D.J., and Lan, H.Y. (2016). TGF-β: the master regulator of fibrosis. Nat. Rev. Nephrol. *12*, 325–338.
7. Wang, X.H., Hu, Z., Klein, J.D., Zhang, L., Fang, F., and Mitch, W.E. (2011). Decreased miR-29 suppresses myogenesis in CKD. J. Am. Soc. Nephrol. *22*, 2068–2076.
8. Papadopoulos, T., Casemayou, A., Neau, E., Breuil, B., Caubet, C., Calise, D., Thornhill, B.A., Bachvarova, M., Belliere, J., Chevalier, R.L., et al. (2017). Systems biology combining human- and animal-data miRNA and mRNA data identifies new targets in ureteropelvic junction obstruction. BMC Syst. Biol. *11*, 31.
9. Guo, J., Yao, H., Lin, X., Xu, H., Dean, D., Zhu, Z., Liu, G., and Sime, P. (2015). IL-13 induces YY1 through the AKT pathway in lung fibroblasts. PLoS ONE *10*, e0119039.
10. Lin, X., Sime, P.J., Xu, H., Williams, M.A., LaRussa, L., Georas, S.N., and Guo, J. (2011). Yin yang 1 is a novel regulator of pulmonary fibrosis. Am. J. Respir. Crit. Care Med. *183*, 1689–1697.
11. Chung, A.C., and Lan, H.Y. (2015). MicroRNAs in renal fibrosis. Front. Physiol. *6*, 50.
12. Qin, W., Chung, A.C., Huang, X.R., Meng, X.M., Hui, D.S., Yu, C.M., Sung, J.J., and Lan, H.Y. (2011). TGF-β/Smad3 signaling promotes renal fibrosis by inhibiting miR-29. J. Am. Soc. Nephrol. *22*, 1462–1474.
13. van Rooij, E., Sutherland, L.B., Thatcher, J.E., DiMaio, J.M., Naseem, R.H., Marshall, W.S., Hill, J.A., and Olson, E.N. (2008). Dysregulation of microRNAs after myocardial infarction reveals a role of miR-29 in cardiac fibrosis. Proc. Natl. Acad. Sci. USA *105*, 13027–13032.
14. Alexander, M., Hu, R., Runtsch, M.C., Kagele, D.A., Mosbruger, T.L., Tolmachova, T., Seabra, M.C., Round, J.L., Ward, D.M., and O'Connell, R.M. (2015). Exosome-delivered microRNAs modulate the inflammatory response to endotoxin. Nat. Commun. *6*, 7321.
15. Wang, X.H. (2013). MicroRNA in myogenesis and muscle atrophy. Curr. Opin. Clin. Nutr. Metab. Care *16*, 258–266.
16. Smyth, T., Kullberg, M., Malik, N., Smith-Jones, P., Graner, M.W., and Anchordoquy, T.J. (2015). Biodistribution and delivery efficiency of unmodified tumor-derived exosomes. J. Control. Release *199*, 145–155.
17. Valadi, H., Ekström, K., Bossios, A., Sjöstrand, M., Lee, J.J., and Lötvall, J.O. (2007). Exosome-mediated transfer of mRNAs and microRNAs is a novel mechanism of genetic exchange between cells. Nat. Cell Biol. *9*, 654–659.
18. Franzen, C.A., Blackwell, R.H., Foreman, K.E., Kuo, P.C., Flanigan, R.C., and Gupta, G.N. (2016). Urinary exosomes: the potential for biomarker utility, intercellular signaling and therapeutics in urological malignancy. J. Urol. *195*, 1331–1339.
19. Robbins, P.D., and Morelli, A.E. (2014). Regulation of immune responses by extracellular vesicles. Nat. Rev. Immunol. *14*, 195–208.
20. Kim, D.K., Lee, J., Kim, S.R., Choi, D.S., Yoon, Y.J., Kim, J.H., Go, G., Nhung, D., Hong, K., Jang, S.C., et al. (2015). EVpedia: a community web portal for extracellular vesicles research. Bioinformatics *31*, 933–939.
21. O'Loughlin, A.J., Woffindale, C.A., and Wood, M.J. (2012). Exosomes and the emerging field of exosome-based gene therapy. Curr. Gene Ther. *12*, 262–274.
22. Wang, B., Zhang, C., Zhang, A., Cai, H., Price, S.R., and Wang, X.H. (2017). MicroRNA-23a and microRNA-27a mimic exercise by ameliorating CKD-induced muscle atrophy. J. Am. Soc. Nephrol. *28*, 2631–2640.
23. Seow, Y., and Wood, M.J. (2009). Biological gene delivery vehicles: beyond viral vectors. Mol. Ther. *17*, 767–777.
24. Hu, Z., Lee, I.H., Wang, X., Sheng, H., Zhang, L., Du, J., and Mitch, W.E. (2007). PTEN expression contributes to the regulation of muscle protein degradation in diabetes. Diabetes *56*, 2449–2456.
25. Zhou, D., and Liu, Y. (2016). Renal fibrosis in 2015: understanding the mechanisms of kidney fibrosis. Nat. Rev. Nephrol. *12*, 68–70.
26. Yu, L., Border, W.A., Huang, Y., and Noble, N.A. (2003). TGF-beta isoforms in renal fibrogenesis. Kidney Int. *64*, 844–856.
27. Zhang, A., Li, M., Wang, B., Klein, J.D., Price, S.R., and Wang, X.H. (2018). miRNA-23a/27a attenuates muscle atrophy and renal fibrosis through muscle-kidney crosstalk. J. Cachexia Sarcopenia Muscle *9*, 755–770.
28. Gilligan, K.E., and Dwyer, R.M. (2017). Engineering exosomes for cancer therapy. Int. J. Mol. Sci. *18*, E1122.
29. Alvarez-Erviti, L., Seow, Y., Yin, H., Betts, C., Lakhal, S., and Wood, M.J. (2011). Delivery of siRNA to the mouse brain by systemic injection of targeted exosomes. Nat. Biotechnol. *29*, 341–345.
30. Masyuk, A.I., Masyuk, T.V., and Larusso, N.F. (2013). Exosomes in the pathogenesis, diagnostics and therapeutics of liver diseases. J. Hepatol. *59*, 621–625.
31. Bivol, L.M., Iversen, B.M., Hultström, M., Wallace, P.W., Reed, R.K., Wiig, H., and Tenstad, O. (2016). Unilateral renal ischaemia in rats induces a rapid secretion of inflammatory markers to renal lymph and increased capillary permeability. J. Physiol. *594*, 1709–1726.
32. Zhou, Q., Du, J., Hu, Z., Walsh, K., and Wang, X.H. (2007). Evidence for adipose-muscle cross talk: opposing regulation of muscle proteolysis by adiponectin and Fatty acids. Endocrinology *148*, 5696–5705.
33. Su, Z., Robinson, A., Hu, L., Klein, J.D., Hassounah, F., Li, M., Wang, H., Cai, H., and Wang, X.H. (2015). Acupuncture plus low-frequency electrical stimulation (Acu-LFES) attenuates diabetic myopathy by enhancing muscle regeneration. PLoS ONE *10*, e0134511.
34. Hu, L., Klein, J.D., Hassounah, F., Cai, H., Zhang, C., Xu, P., and Wang, X.H. (2015). Low-frequency electrical stimulation attenuates muscle atrophy in CKD—a potential treatment strategy. J. Am. Soc. Nephrol. *26*, 626–635.
35. Su, Z., Klein, J.D., Du, J., Franch, H.A., Zhang, L., Hassounah, F., Hudson, M.B., and Wang, X.H. (2017). Chronic kidney disease induces autophagy leading to dysfunction of mitochondria in skeletal muscle. Am. J. Physiol. Renal Physiol. *312*, F1128–F1140.
36. Du, J., Klein, J.D., Hassounah, F., Zhang, J., Zhang, C., and Wang, X.H. (2014). Aging increases CCN1 expression leading to muscle senescence. Am. J. Physiol. Cell Physiol. *306*, C28–C36.
37. Hu, Z., Klein, J.D., Mitch, W.E., Zhang, L., Martinez, I., and Wang, X.H. (2014). MicroRNA-29 induces cellular senescence in aging muscle through multiple signaling pathways. Aging (Albany N.Y.) *6*, 160–175.

YMTHE, Volume *27*

Supplemental Information

Exosome-Mediated miR-29 Transfer Reduces Muscle Atrophy and Kidney Fibrosis in Mice

Haidong Wang, Bin Wang, Aiqing Zhang, Faten Hassounah, Yiqi Seow, Matthew Wood, Fuying Ma, Janet D. Klein, S. Russ Price, and Xiaonan H. Wang

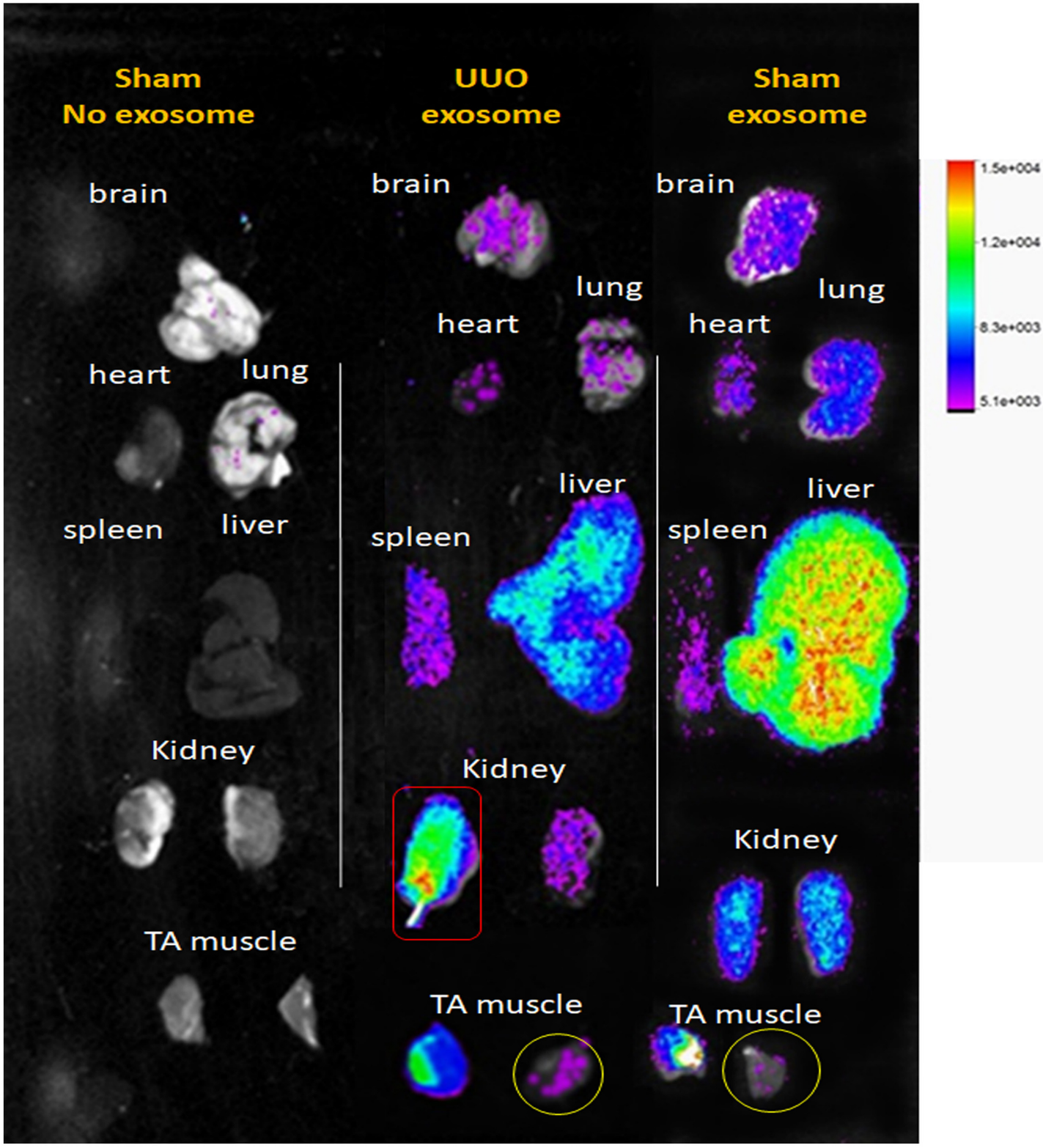

Supplement Figure 1: the fluorescently labeled Exo/miR -29 distribution in organs following intramuscular injection. Mice were injected in the left TA muscle with Exo/miR-29 labeled with1 μmol/l fluorescent lipophilic tracer DiR at the same time as UUO surgery. The injection was repeat once per week. Shown are representative fluorescent organs images at 14 -days that were acquired using a Bruker Small Animal Optical Imaging System. Panels from left to right: Sham operated with no exosome/DiR injection, UUO mouse with exosome/DiR injection at 14 -days and sham operated with exosome injection. The UUO kidney is in red square and the right TA that did not receive any injection is designated within a yellow circle.

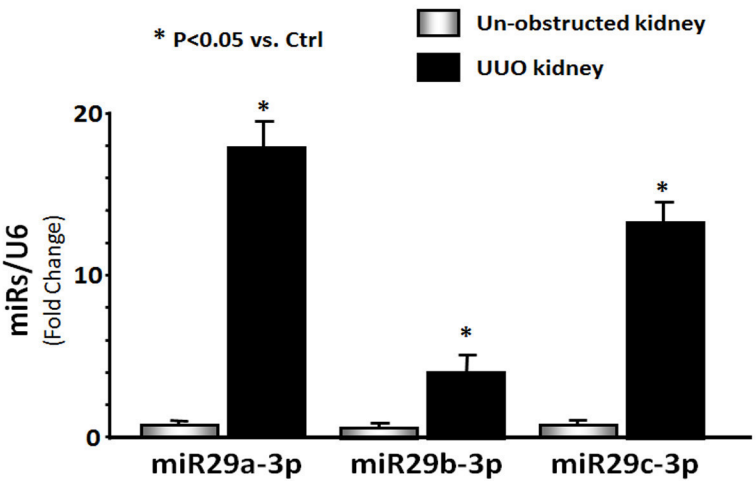

Supplement Figure 2: the increase of miR-29 in the obstructed kidney was more than in the unobstructed kidney. The expression of miR-29a-3p, miR-29b-3p and miR-29c-3p were assayed by real time qPCR in UUO mice. The bar graph shows miR-29s expression from the obstructed kidney compared with levels in non-obstructed kidney (represented by 1-fold). Results are normalized to U6. (Bars: mean ± s.e.; n=6/group; *=p<0.05 vs. Exo/ctrl). The expression of miR-29a, b and c was increased in the obstructed kidney by 18-, 4- and 13-fold, respectively.

(A)

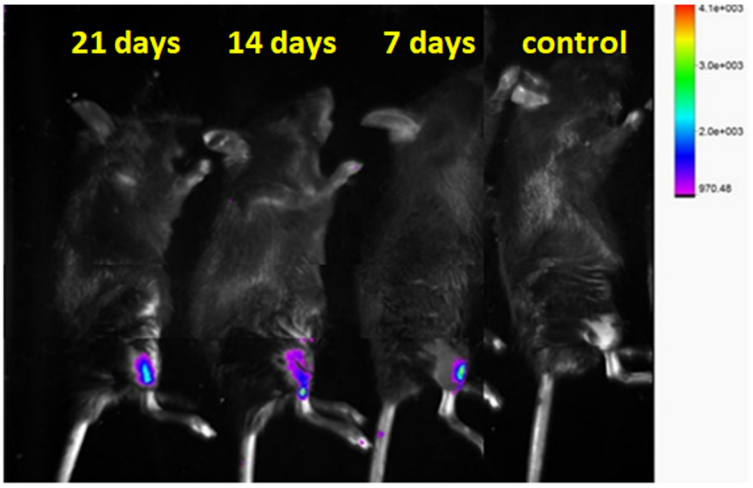

(B)

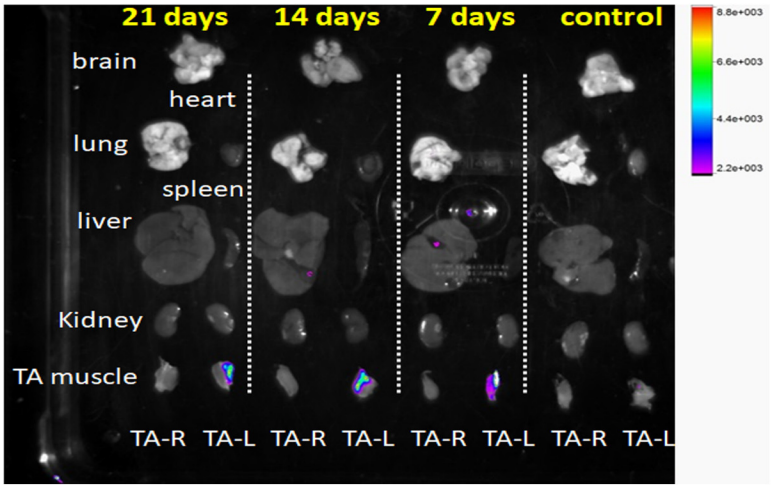

Supplement Figure 3: injection of the DiR only into the left TA muscle did not result in multiple organ distribution. Supplement Figure 3: injection of the DiR only into the left TA muscle did not result in multiple organ distribution. The fluorescence distribution was determined in muscle and organs at 7, 14 and 21 days after intramuscular injection of DiR without exosome and microRNA in normal mice. (A) Images were taken of whole mice; the right control mouse did not receive any DiR injection. (B) Each organ was removed from the mice that received intramuscular injection of DiR in the left TA muscle.

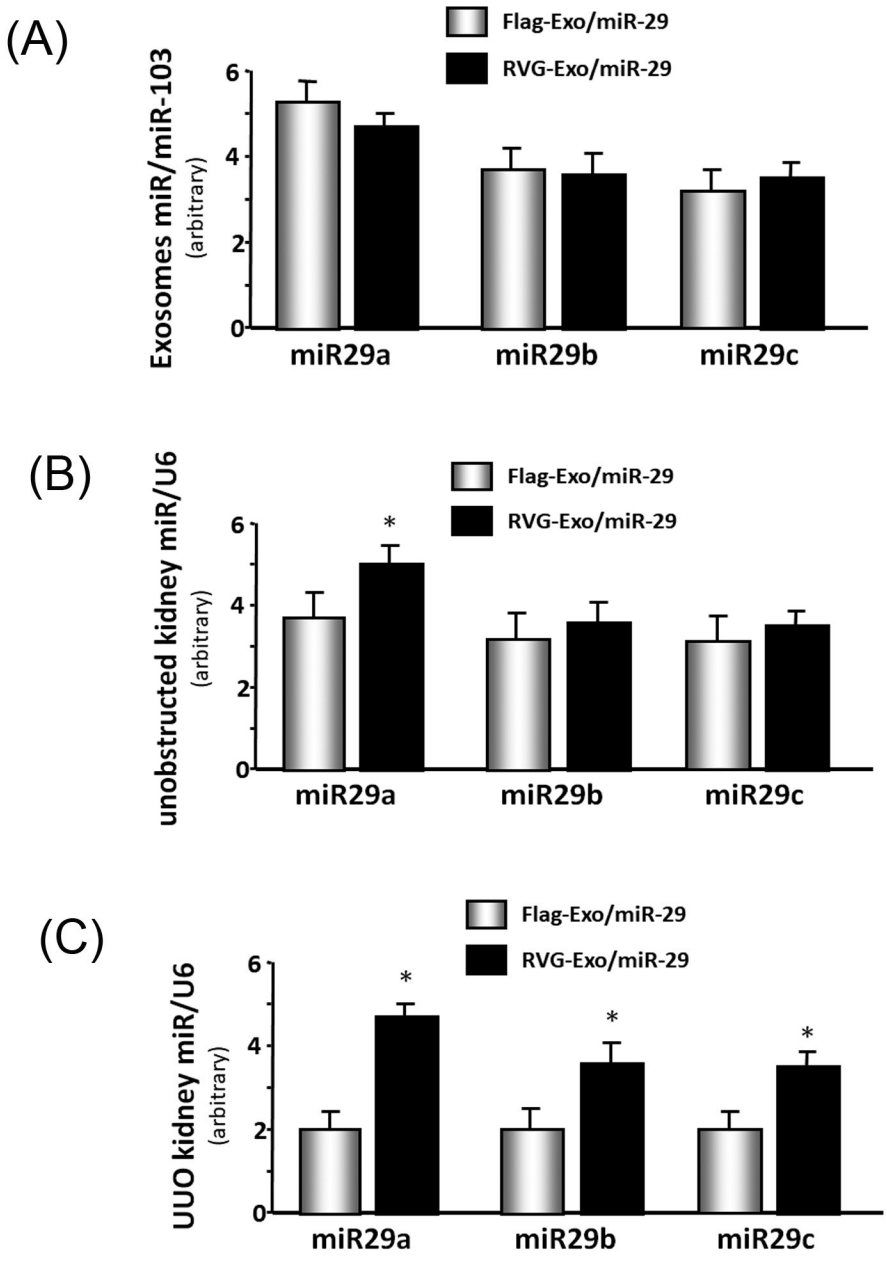

Supplement Figure 4: Compare the miR-29 expression in Flag-Exo/miR-29 and RVG-Exo/miR-29 injected mice. (A) RNA was isolated from serum exosome of UUO mice. (B) RNA was isolated from un-obstructive kidney of UUO mice. (C) RNA was isolated from obstructive kidney of UUO mice. The expression of miR-29a-3p, miR-29b-3p and miR-29c-3p were assayed by real time qPCR. The bar graph shows miR expression in an arbitrary unit. Results are normalized to miR-103 (serum) or U6 (kidney). (Bars: mean ± s.e.; n=6/group; *=$p<0.05$ vs. Flag-Exo/miR-29).

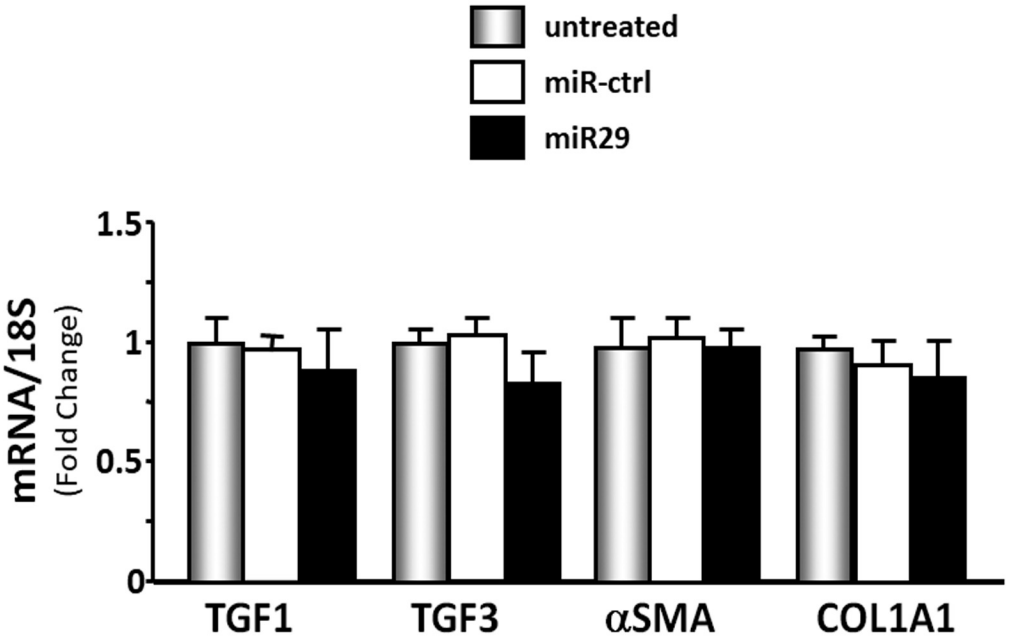

Supplementary Figure 5: Compare the mRNA expression in miR-control, miR-miR-29 and untreated HEK293 cells. Cultured cells were treated with Ad-miR-ctrl (miR-ctrl), Ad-miR29 (miR29), and untreated. Total RNA was extracted from the cells 24 hours after treatment. The expression of TGF-β1, TGF-β3, α-SMA and collagen 1A1 (COL1A1) were assayed by real time qPCR. The bar graph shows mRNA from the cells of each group compared with levels in untreated. Results are normalized to 18S (Bars: mean ± s.e.; n=4/group).

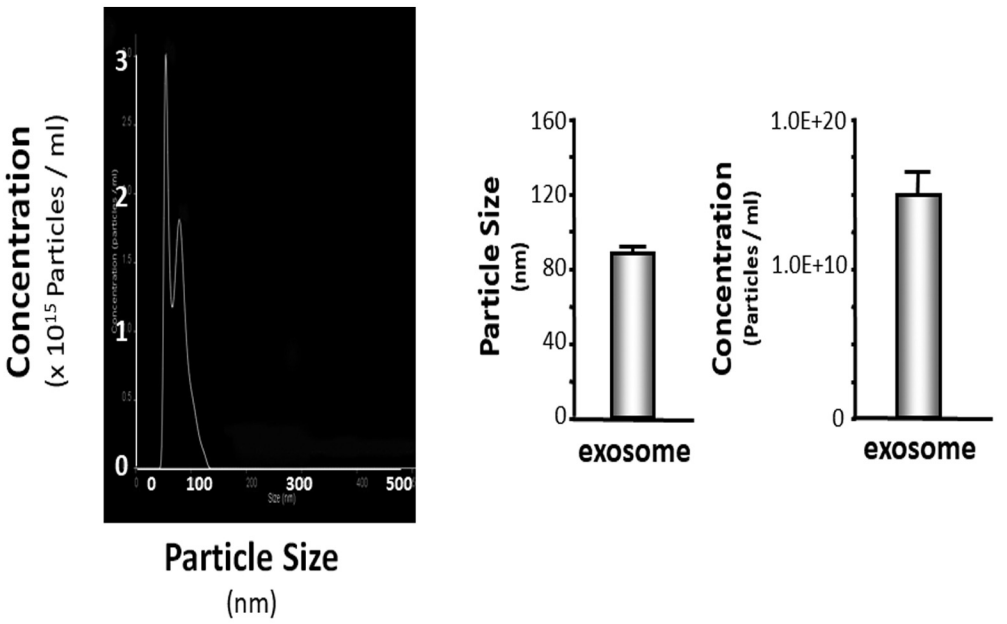

Supplementary Figure 6: The size and concentration of exosomes isolated from satellite cell culture medium. The exosome size and concentration was measured a NanoSight instrument. The bar graphs shows the size (x axis, nanometer diameter) and concentration (Y axis, Particles / ml) of exosomes from serum of 3 of mice (Bars: mean ± s.e.; n=3/group).

Supplementary Materials and Methods

Animals and unilateral ureteral obstruction (UUO) Model: These experiments were approved by the Emory University IACUC (protocol 141-2008). The mice (C57BL/6J) were from Jackson Laboratories (Bar Harbor, ME, USA) and were housed with a 12-hour light/12-hour dark cycle. For UUO surgery, mice were anesthetized with intraperitoneal injection of a combination of 12 mg/kg xylazine and 60 mg/kg ketamine and were placed in a prone position. An incision was made in skin and subcutaneous tissue along the length of the 11th rib using scissors. Muscles were divided and pleura was carefully pushed upward, exposing the kidney. The left ureter was visualized and ligated with 4-0 silk at two points just below the lower pole of the left kidney. The ureter was cut between the two ligatures in order to prevent retrograde urinary tract infection. The sham operation consisted of a similar incision and identification of the left ureter, but no ligation of the ureter was performed. The mice were terminated at 3, 7, 14 and 30 days after the UUO operation. Blood urea nitrogen (BUN) was measured with a BUN Kinetic Procedure Kit (Thermo Electron, Louisville, CO.).

Generation of exosome encapsulated miR-29a: Satellite cells were grown to 60% confluence in DMEM/F12 culture medium containing 20% fetal bovine serum. The Lamp2b-RVG vector was transfected into satellite cells using the Effectene transfection reagent (Qiagen, Valencia, CA). Six hours after transfection, the cells were transduced with Ad-miR29abc (adenovirus containing miR-29ab1 and -b2c precursor sequences)[1]. Control cells were transduced with Ad-empty for production of RVG-exosome-control (Exo/ctrl). 24 hours after transfection/transduction the culture medium was exchanged for a medium with extracellular vesicle free serum (EVFS) and cultured for an additional 48 hours to allow exosomes to be released into the medium. The RVG-exosomes enriched with miR-29abc (Exo/miR29) were harvested from culture medium and re-suspended in PBS (supplement Figure 4). The increased expression of miR-29a, b and c in the exosomes was assayed by qPCR (Figure 2A). The yield of exosomes from the culture medium, approximately 1.5×10^{15} particles/ml, was determined using a NanoSight instrument measurement (Figure 2A). Previously study showed that RVG is located on external exosome membrane[37].

Exosome isolation, NanoSight measurement and in vivo imaging: To isolate exosomes, cell debris and non-exosome organelles were removed from either serum (diluted 5x with PBS) or culture medium (undiluted) by centrifugation at 1,000 g for 10 min, 4^{o}C. The supernatant fraction

was further centrifuged at 16,000 g for 30 min, 4°C. This second supernatant was sterile filtered through a 0.22 μm filter. Exosomes were pelleted from this filtrate at 120,000 g for 90 min at 4°C (L8-70M ultracentrifuge, Beckman-Coulter, Indianapolis IN). Exosome pellets were re-suspended in PBS and protein was quantified using a Bradford protein assay (Bio-Rad, Hercules, CA). Exosome concentration and size (Figure 2B) were measured using nanoparticle tracking analysis (NanoSight NS300, Malvern Instruments, Inc. Westborough, MA). The exosomal protein marker, TSG101, was assessed by Western blot (Figure 2C). *In vivo* exosome distribution was determined with the Bruker Small Animal Optical Imaging System (In-Vivo Xtreme II; Billerica, MA).

Culture of primary muscle satellite cells and HEK293 cells: Satellite cells were isolated from the hindlimb muscles of 4-month old mice. A Skeletal Muscle Dissociation Kit (130-098-305; MACS, Miltenyi Biotec, Inc. Auburn, CA) was used to dissociate mouse skeletal muscle tissue into cell suspensions and a Satellite Cell Isolation Kit (130-104-267, MACS) was used to isolate satellite cells. Cells were cultured in Ham's F-10 Nutrient Mixture medium (Invitrogen) with 20% fetal bovine serum, 100 u/ml penicillin, 100 μg/ml streptomycin (growth medium). Isolated satellite cells were passaged a maximum of 5 times. Myotube differentiation was inhibited by the addition of 5ng/ml human β-fibroblast growth factor (FGF, Atlanta Biologicals, Atlanta, GA) to the media. FGF was removed for 2 days before the experiments to allow myotubes formation. Satellite cells were stained with anti-eMyHC or anti-α-smooth muscle actin (Sigma) to verify the purity of the culture [2]. To stimulate fibrosis in cultured cells, cells were treated with 10ng/ml recombinant human TGF-β purchased from R&D Systems (Cat# 240-B/CF) for 48h. We re-probe every single western blot membrane with GAPDH. In general, we did not strip the membrane. Primary antibody protein bands were scanned and quantified using the Li-COR Odyssey infrared scanning system (Li-COR Biosciences, Lincoln, Nebraska). Then the blot is reprobed with GAPDH antibody and GAPDH density is determined, again using the Li-COR system. When the primary protein has a very different molecular weight from GAPDH there is no overlap and no adjustments are needed. Usually even if the first antibody is close in molecular weight to GAPDH, the density of the first antibody is tiny compared with the response of GAPDH, so any underlying density if minimal, but since we have the signal of the underlying band, we can subtract it from the GAPDH band which allows us to use GAPDH as a loading control. In the event of an unusually strong first antibody response, we 1) strip the membrane and then probe for GAPDH, or 2) use a different host antibody (ie, rabbit Ab first, mouse Ab GAPDH) which allows

us to use a secondary antibody with a different wavelength fluorescent moiety so the overlap does not contribute to the signal. We showed a representative GAPDH response that we routinely see, but think it too cumbersome to provide the GAPDH bands for each protein probed.

Western blot and antibodies: Hind limb muscle were homogenized in Gentle Lysis Buffer (10 mM Tris-HCl, 10 mM NaCl, 2 mM EDTA, 0.5 % NP-40, 1 % glycerol, and fresh added: 1 mM Na3VO4; 10μg/ml PMSF; 5μg/ml Aprotinin; 1μg/ml Leupeptin) with phosphatase inhibitors cocktail 1 and 2 (Sigma) [3, 4]. Protein concentration was measured using a RC-PC protein assay kit (Bio-Rad). Equal amounts of protein were loaded on the acrylamide/bis SDS-PAGE gel. We used 50 micrograms for exosome protein loading, and 20 micrograms for the skeletal muscle and kidney. Protein was transferred to a PVDF membrane and blotted with a specific primary antibody. The secondary antibodies that we used included Alexa Fluor® 680 goat anti-Rabbit IgG or goat anti-mouse IgG are from Invitrogen (Carlsbad, CA). Protein bands were scanned and quantified using the Li-cor Odyssey infrared scanning system (Li-COR Biosciences, Lincoin, Nebraska).

RNA extraction and quantitative real-time PCR: Total RNA from muscle and kidney were extracted using Tri-Reagent (Molecular Research Inc., Cincinnati, OH). Exosomal RNA was isolated using a miRNAeasy kit (217004, Qiagen Sciences, Germantown, MD) and quantified using a NanoDrop spectrophotometer (Thermo Scientific, Wilmington, DE). For mRNA expression, total RNA (1-2 μg) was reverse transcribed using a Thermoscript RT-PCR kit (Invitrogen Carlsbad, CA). Real-time qPCR was performed with the SYBR Green PCR reagent (Bio-Rad) and the following PCR parameters: 94°C for 2 minutes and 40 cycles at 94°C for 15 seconds, 55°C for 30 seconds, 72°C for 30 seconds with final extension at 72°C for 10 minutes[5, 6]. The Cq (threshold cycle) was defined as the number of cycles required for the fluorescence signal to exceed the detection threshold. Individual mRNA expression was standardized to 18S gene and expression was calculated as the difference between the threshold values of the two genes (ΔΔcq). Melting curve analysis was always performed during real-time qPCR to analyze and verify the specificity of the reaction. Primers for mRNA are listed in Table 2. For microRNA, RNA was reverse transcribed using a universal cDNA synthesis kit II (cat #203301 Exiqon, Wobum, MA). The primers were purchased from Exiqon. Real-time qPCR was performed with the ExiLENT SYBR green master mix (Exiqon cat# 203421). Expression of individual miR-29a-3p, miR-29b-3p and miR-29c-3p in muscle and kidney tissue were normalized to the mouse U6

mRNA and calculated as the difference between the threshold values of the two genes (ΔΔcq). The expression of individual miRs in serum exosomes was normalized to miR-103a.

Muscle and kidney histology: Tissues were fixed in 3.7% formaldehyde/PBS (pH 7.4), and dehydrated, paraffin embedded and sectioned. Masson trichromatic staining was performed with a Masson modified IMEB stain kit (K7298, IMEB Inc. San Marcos, CA). Images were visualized with an Olympus 1X 51 inverted microscopes and captured by DP73-1-51-17MP color camera. Collagen (blue color) in kidney was measured using the CellSens Dimension 1.9 Software (Olympus, Melville, NY, USA) and color density calculated as the average from 10 individual fields.

For skeletal muscle immunohistology: muscles were embedded in Tissue Freezing Media (Cat# H-TFM; Fisher, Pittsburgh, PA, USA) by immersing in isopentane cooled in dry ice. Cross sections (10 mm) from the mid-belly of different muscles were mounted on gelatin-coated slides and fixed in 4% paraformaldehyde for 10 min. Tissue was permeabilized in 0.05% Triton X-100 (in PBS) for 10 min, and quench-fixed in 50 mM NH_4Cl for another 10 min. Samples were blocked with 5% bovine serum albumin for 1 h, followed by incubation overnight with primary antibody. Sections were subsequently washed with PBS and incubated for 60 min with FITC-labeled anti-rabbit IgG (111-095-144; diluted 1:100; Jackson Immuno Research Lab, West Grove, PA). Nuclei were stained by DAPI. Images were visualized with an Olympus 1X51 inverted fluorescence microscope and captured by DP73-1-51-17MP color camera. Muscle fiber cross-sectional area was determined in TA using an anti-laminin antibody (1:50 dilution; Sigma-Aldrich) and at least 500 individual myofibers per muscle were measured. Kidneys dehydrated with increasing concentrations of sucrose, then embedded in tissue freezing medium and frozen in liquid N_2. Sections (10 micron) were cut, mounted on slides and stained with primary antibodies as described for muscle above.

Luciferase reporter assay and transfection: Effectene transfection reagent was used for transfection (Qiagen, Valencia, CA). Firefly and Renilla luciferase activities were measured by dual-luciferase assays (Promega) using TD-20/20 Luminometer (Turner designs, Sunnyvale, CA) [7]. The luciferase report vectors (pMIR-REPORT Luciferase) were purchase from Applied BIOSYSTEMS (Waltham, MA) and constructs were made by Emory Integrated Genomics Core.

Statistical analysis: Data were presented as mean ± se. To identify significant differences between two groups, comparisons were made by using the Student's t-test. When multiple

treatments were compared, ANOVA was performed with a post hoc analysis by the Student-Newman-Keuls test. The relationship between muscle and kidney fluorescence intensity was calculated by linear regression modeling. Differences with P values < 0.05 were considered significant.

Reference:

1. Wang XH, Hu Z, Klein JD, *et al.* Decreased miR-29 suppresses myogenesis in CKD. *J Am Soc Nephrol* 2011; **22:** 2068-2076.

2. Wang B, Zhang C, Zhang A, *et al.* MicroRNA-23a and MicroRNA-27a Mimic Exercise by Ameliorating CKD-Induced Muscle Atrophy. *J Am Soc Nephrol* 2017.

3. Zhou Q, Du J, Hu Z, *et al.* Evidence for adipose-muscle cross talk: opposing regulation of muscle proteolysis by adiponectin and Fatty acids. *Endocrinology* 2007; **148:** 5696-5705.

4. Su Z, Robinson A, Hu L, *et al.* Acupuncture plus Low-Frequency Electrical Stimulation (Acu-LFES) Attenuates Diabetic Myopathy by Enhancing Muscle Regeneration. *PLoS One* 2015; **10:** e0134511.

5. Su Z, Hu L, Cheng J, *et al.* Acupuncture plus Low-Frequency Electrical Stimulation (Acu-LFES) attenuates denervation-induced muscle atrophy. *J Appl Physiol (1985)* 2015**:** jap 00175 02015.

6. Hu L, Klein JD, Hassounah F, *et al.* Low-Frequency Electrical Stimulation Attenuates Muscle Atrophy in CKD-A Potential Treatment Strategy. *J Am Soc Nephrol* 2015; **26:** 626-635.

7. Du J, Klein JD, Hassounah F, *et al.* Aging increases CCN1 expression leading to muscle senescence. *Am J Physiol Cell Physiol* 2014; **306:** C28-36.